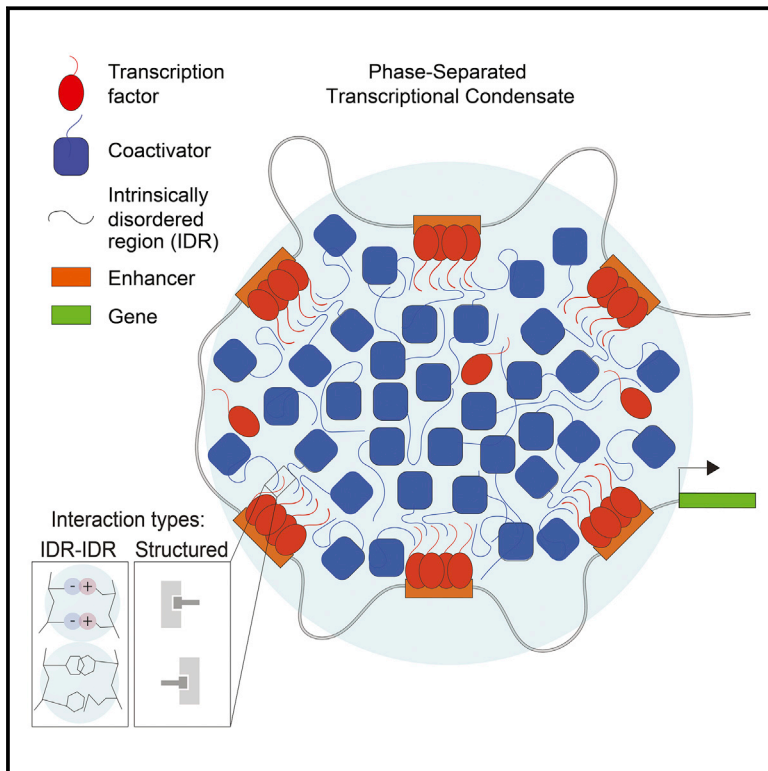


Transcription Factors Activate Genes through the Phase-Separation Capacity of Their Activation Domains

Graphical Abstract



Authors

Ann Boija, Isaac A. Klein, Benjamin R. Sabari, ..., Tong Ihn Lee, Dylan J. Taatjes, Richard A. Young

Correspondence

young@wi.mit.edu

In Brief

Activation domains from a diverse array of mammalian and yeast transcription factors form phase-separated condensates with Mediator to activate gene expression.

Highlights

- Transcription factors (TFs) form phase-separated condensates with Mediator
- Phase separation of activation domains is a general property of TFs
- Phase-separation capacity of TFs is associated with gene activation
- TF condensates incorporate dynamic and structured interactions

Transcription Factors Activate Genes through the Phase-Separation Capacity of Their Activation Domains

Ann Boija,^{1,7} Isaac A. Klein,^{1,2,7} Benjamin R. Sabari,¹ Alessandra Dall'Agnese,¹ Eliot L. Coffey,^{1,3} Alicia V. Zamudio,^{1,3} Charles H. Li,^{1,3} Krishna Shrinivas,^{4,5} John C. Manteiga,^{1,3} Nancy M. Hannett,¹ Brian J. Abraham,¹ Lena K. Afeyan,^{1,3} Yang E. Guo,¹ Jenna K. Rimel,⁶ Charli B. Fant,⁶ Jurian Schuijers,¹ Tong Ihn Lee,¹ Dylan J. Taatjes,^{6,8} and Richard A. Young^{1,3,8,9,*}

¹Whitehead Institute for Biomedical Research, Cambridge, MA 02142, USA

²Department of Medical Oncology, Dana-Farber Cancer Institute, Harvard Medical School, Boston, MA 02215, USA

³Department of Biology, Massachusetts Institute of Technology, Cambridge, MA 02139, USA

⁴Department of Chemical Engineering, Massachusetts Institute of Technology, Cambridge, MA 02139, USA

⁵Institute of Medical Engineering and Science, Massachusetts Institute of Technology, Cambridge, MA 02139, USA

⁶Department of Biochemistry, University of Colorado, Boulder, CO 80303, USA

⁷These authors contributed equally

⁸Senior author

⁹Lead Contact

*Correspondence: young@wi.mit.edu

<https://doi.org/10.1016/j.cell.2018.10.042>

SUMMARY

Gene expression is controlled by transcription factors (TFs) that consist of DNA-binding domains (DBDs) and activation domains (ADs). The DBDs have been well characterized, but little is known about the mechanisms by which ADs effect gene activation. Here, we report that diverse ADs form phase-separated condensates with the Mediator coactivator. For the OCT4 and GCN4 TFs, we show that the ability to form phase-separated droplets with Mediator *in vitro* and the ability to activate genes *in vivo* are dependent on the same amino acid residues. For the estrogen receptor (ER), a ligand-dependent activator, we show that estrogen enhances phase separation with Mediator, again linking phase separation with gene activation. These results suggest that diverse TFs can interact with Mediator through the phase-separating capacity of their ADs and that formation of condensates with Mediator is involved in gene activation.

INTRODUCTION

Regulation of gene expression requires that the transcription apparatus be efficiently assembled at specific genomic sites. DNA-binding transcription factors (TFs) ensure this specificity by occupying specific DNA sequences at enhancers and promoter-proximal elements. TFs typically consist of one or more DNA-binding domains (DBDs) and one or more separate activation domains (ADs) (Brent and Ptashne, 1985; Keegan et al., 1986). While the structure and function of TF DBDs are well documented, comparatively little is understood about the struc-

ture of ADs and how these interact with coactivators to drive gene expression.

The structure of TF DBDs and their interaction with cognate DNA sequences has been described at atomic resolution for many TFs, and TFs are generally classified according to the structural features of their DBDs (Fulton et al., 2009; Vaquerizas et al., 2009). For example, DBDs can be composed of zinc-coordinating, basic helix-loop-helix, basic-leucine zipper, or helix-turn-helix DNA-binding structures. These DBDs selectively bind specific DNA sequences that range from 4 to 12 bp, and the DNA binding sequences favored by hundreds of TFs have been described (Hume et al., 2015; Jolma et al., 2013; Khan et al., 2018). Multiple TF molecules typically bind together at any one enhancer or promoter-proximal element. For example, at least eight different TF molecules bind a 50-bp core component of the interferon (IFN)- β enhancer (Panne et al., 2007).

Anchored in place by the DBD, the AD interacts with coactivators, which integrate signals from multiple TFs to regulate transcriptional output (Allen and Taatjes, 2015; Juven-Gershon and Kadonaga, 2010; Malik and Roeder, 2010; Plaschka et al., 2016; Reiter et al., 2017; Soutourina, 2018; Taatjes, 2010). In contrast to the structured DBD, the ADs of most TFs are low-complexity amino acid sequences not amenable to crystallography. These intrinsically disordered regions (IDRs) have therefore been classified by their amino acid profile as acidic, proline, serine/threonine, or glutamine rich or by their hypothetical shape as acid blobs, negative noodles, or peptide lassos (Mitchell and Tjian, 1989; Roberts, 2000; Sigler, 1988; Staby et al., 2017; Triezenberg, 1995). Remarkably, hundreds of TFs are thought to interact with the same small set of coactivator complexes, which include Mediator and p300 (Allen and Taatjes, 2015; Avantaggiati et al., 1996; Dai and Markham, 2001; Eckner et al., 1996; Green, 2005; Merika et al., 1998; Oliner et al., 1996; Yin and Wang, 2014; Yuan et al., 1996). ADs that share little

sequence homology are functionally interchangeable among TFs (Godowski et al., 1988; Hope and Struhl, 1986; Jin et al., 2016; Lech et al., 1988; Ransone et al., 1990; Sadowski et al., 1988; Struhl, 1988; Tora et al., 1989); this interchangeability is not readily explained by traditional lock-and-key models of protein-protein interaction. Thus, how the diverse ADs of hundreds of different TFs interact with a similar small set of coactivators remains a conundrum.

Recent studies have shown that the AD of the yeast TF GCN4 binds to the Mediator subunit MED15 at multiple sites and in multiple orientations and conformations (Brzovic et al., 2011; Jedidi et al., 2010; Tuttle et al., 2018; Warfield et al., 2014). The products of this type of protein-protein interaction, where the interaction interface cannot be described by a single conformation, have been termed “fuzzy complexes” (Tompa and Fuxreiter, 2008). These dynamic interactions are also typical of the IDR-IDR interactions that facilitate formation of phase-separated biomolecular condensates (Alberti, 2017; Banani et al., 2017; Hyman et al., 2014; Shin and Brangwynne, 2017; Wheeler and Hyman, 2018).

We recently proposed that transcriptional control may be driven by the formation of phase-separated condensates (Hnisz et al., 2017) and demonstrated that the coactivator proteins MED1 and BRD4 form phase-separated condensates at super-enhancers (SEs) (Sabari et al., 2018). Here, we report that diverse TF ADs phase separate with the Mediator coactivator. We show that the embryonic stem cell (ESC) pluripotency TF OCT4, the estrogen receptor (ER), and the yeast TF GCN4 form phase-separated condensates with Mediator and require the same amino acids or ligands for both activation and phase separation. We propose that IDR-mediated phase separation with coactivators is a mechanism by which TF ADs activate genes.

RESULTS

Mediator Condensates at ESC SEs Depend on OCT4

OCT4 is a master TF essential for the pluripotent state of ESCs and is a defining TF at ESC SEs (Whyte et al., 2013). The Mediator coactivator, which forms condensates at ESC SEs (Sabari et al., 2018), is thought to interact with OCT4 via the MED1 subunit (Table S1) (Apostolou et al., 2013). If OCT4 contributes to the formation of Mediator condensates, then OCT4 puncta should be present at the SEs where MED1 puncta have been observed. Indeed, immunofluorescence (IF) microscopy with concurrent nascent RNA fluorescence in situ hybridization (FISH) revealed discrete OCT4 puncta at the SEs of the key pluripotency genes *Esrrb*, *Nanog*, *Trim28*, and *Mir290* (Figure 1). Average image analysis confirmed that OCT4 IF was enriched at center of RNA FISH foci. This enrichment was not seen using a randomly selected nuclear position (Figure S1). These results confirm that OCT4 occurs in puncta at the same SEs where Mediator forms condensates (Sabari et al., 2018) and where chromatin immunoprecipitation sequencing (ChIP-seq) shows co-occupancy of OCT4 and MED1 (Figure 1).

We investigated whether the Mediator condensates present at SEs are dependent on OCT4 using a degradation strategy (Nabet et al., 2018). Degradation of OCT4 in an ESC line bearing

endogenous knockin of DNA encoding the FKBP protein fused to OCT4 was induced by addition of dTag for 24 hr (Weintraub et al., 2017) (Figures 2A and S2A). Induction of OCT4 degradation reduced OCT4 protein levels but did not affect MED1 levels (Figure S2B). ChIP-seq analysis showed a reduction of OCT4 and MED1 occupancy at enhancers, with the most profound effects occurring at SEs, as compared to typical enhancers (TEs) (Figure 2B). RNA sequencing (RNA-seq) revealed that expression of SE-driven genes was concomitantly decreased (Figure 2B). For example, OCT4 and MED1 occupancy was reduced by approximately 90% at the *Nanog* SE (Figure 2C), associated with a 60% reduction in *Nanog* mRNA levels (Figure 2D). IF microscopy with concurrent DNA FISH showed that OCT4 degradation caused a reduction in MED1 condensates at *Nanog* (Figures 2E and S2C). These results indicate that the presence of Mediator condensates at an ESC SE is dependent on OCT4.

ESC differentiation causes a loss of OCT4 binding at certain ESC SEs, which leads to a loss of these OCT4-dependent SEs, and thus should cause a loss of Mediator condensates at these sites. To test this idea, we differentiated ESCs by leukemia inhibitory factor (LIF) withdrawal. In the differentiated cell population, we observed reduced OCT4 and MED1 occupancy at the *Mir290* SE (Figures 2F, 2G, and S2D) and reduced levels of *Mir290* miRNA (Figure 2H), despite continued expression of MED1 protein (Figure S2E). Correspondingly, MED1 condensates were reduced at *Mir290* (Figures 2I and S2F) in the differentiated cell population. These results are consistent with those obtained with the OCT4 degron experiment and support the idea that Mediator condensates at these ESC SEs are dependent on occupancy of the enhancer elements by OCT4.

OCT4 Is Incorporated into MED1 Liquid Droplets

OCT4 has two intrinsically disordered ADs responsible for gene activation, which flank a structured DBD (Figure 3A) (Brehm et al., 1997). Since IDRs are capable of forming dynamic networks of weak interactions, and the purified IDRs of proteins involved in condensate formation can form phase-separated droplets (Burke et al., 2015; Lin et al., 2015; Nott et al., 2015), we next investigated whether OCT4 is capable of forming droplets *in vitro*, with and without the IDR of the MED1 subunit of Mediator.

Recombinant OCT4-GFP fusion protein was purified and added to droplet formation buffers containing a crowding agent (10% PEG-8000) to simulate the densely crowded environment of the nucleus. Fluorescent microscopy of the droplet mixture revealed that OCT4 alone did not form droplets throughout the range of concentrations tested (Figure 3B). In contrast, purified recombinant MED1-IDR-GFP fusion protein exhibited concentration-dependent liquid-liquid phase separation (Figure 3B), as described previously (Sabari et al., 2018).

We then mixed the two proteins and found that droplets of MED1-IDR incorporate and concentrate purified OCT4-GFP to form heterotypic droplets (Figure 3C). In contrast, purified GFP was not concentrated into MED1-IDR droplets (Figures 3C and S3A). OCT4-MED1-IDR droplets were near micrometer sized (Figure S3B), exhibited fast recovery after photobleaching (Figure 3D), had a spherical shape (Figure S3C), and were salt

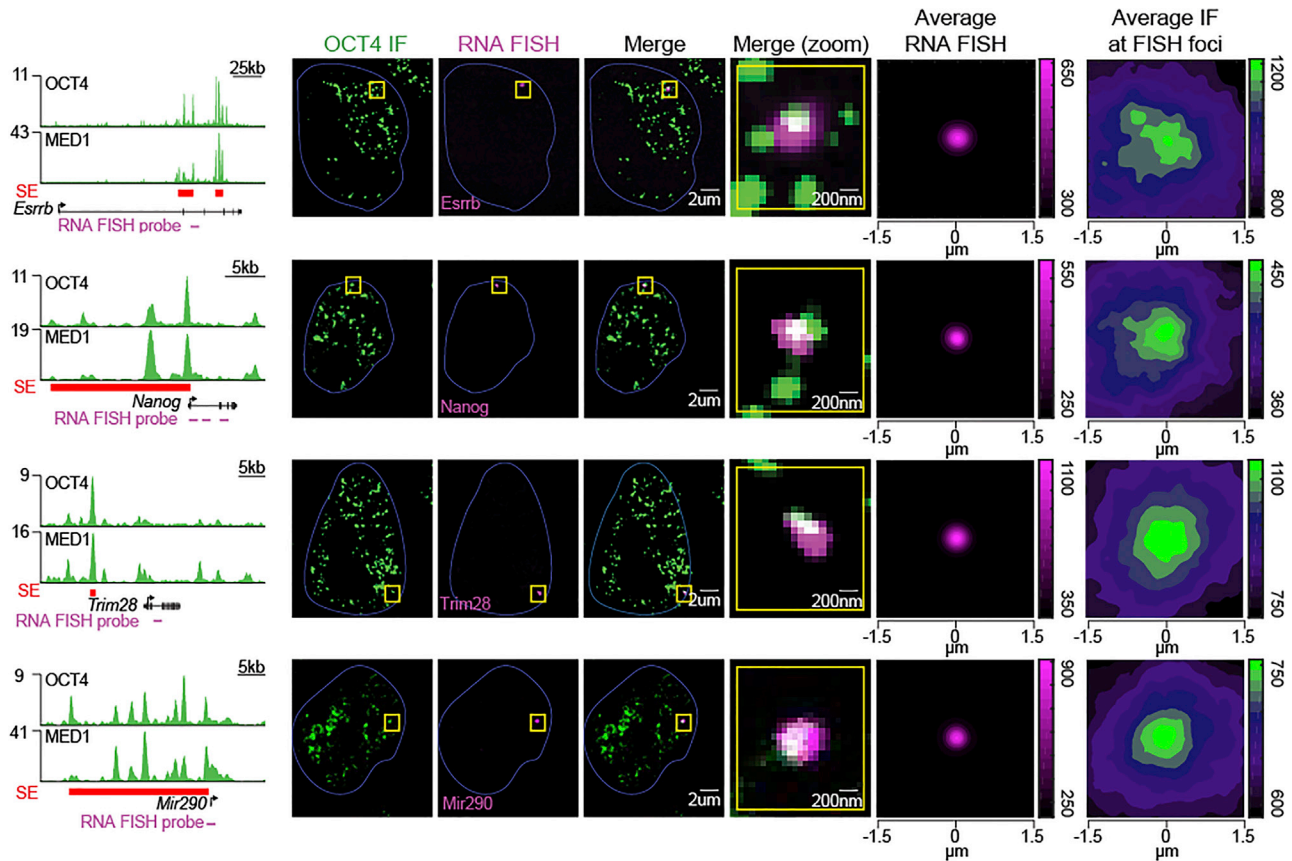


Figure 1. OCT4 and Mediator Occupy SEs In Vivo

ChIP-seq tracks of OCT4 and MED1 in ESCs at SEs (left column) and OCT4 IF with concurrent RNA-FISH demonstrating occupancy of OCT4 at *Esrrb*, *Nanog*, *Trim28*, and *Mir290*. Hoechst staining was used to determine the nuclear periphery, highlighted with a blue line. The two rightmost columns show average RNA FISH signal and average OCT4 IF signal centered on the RNA-FISH focus from at least 11 images. Average OCT4 IF signal at a randomly selected nuclear position is displayed in Figure S1.

See also Figure S1 and Tables S1, S2, and S4.

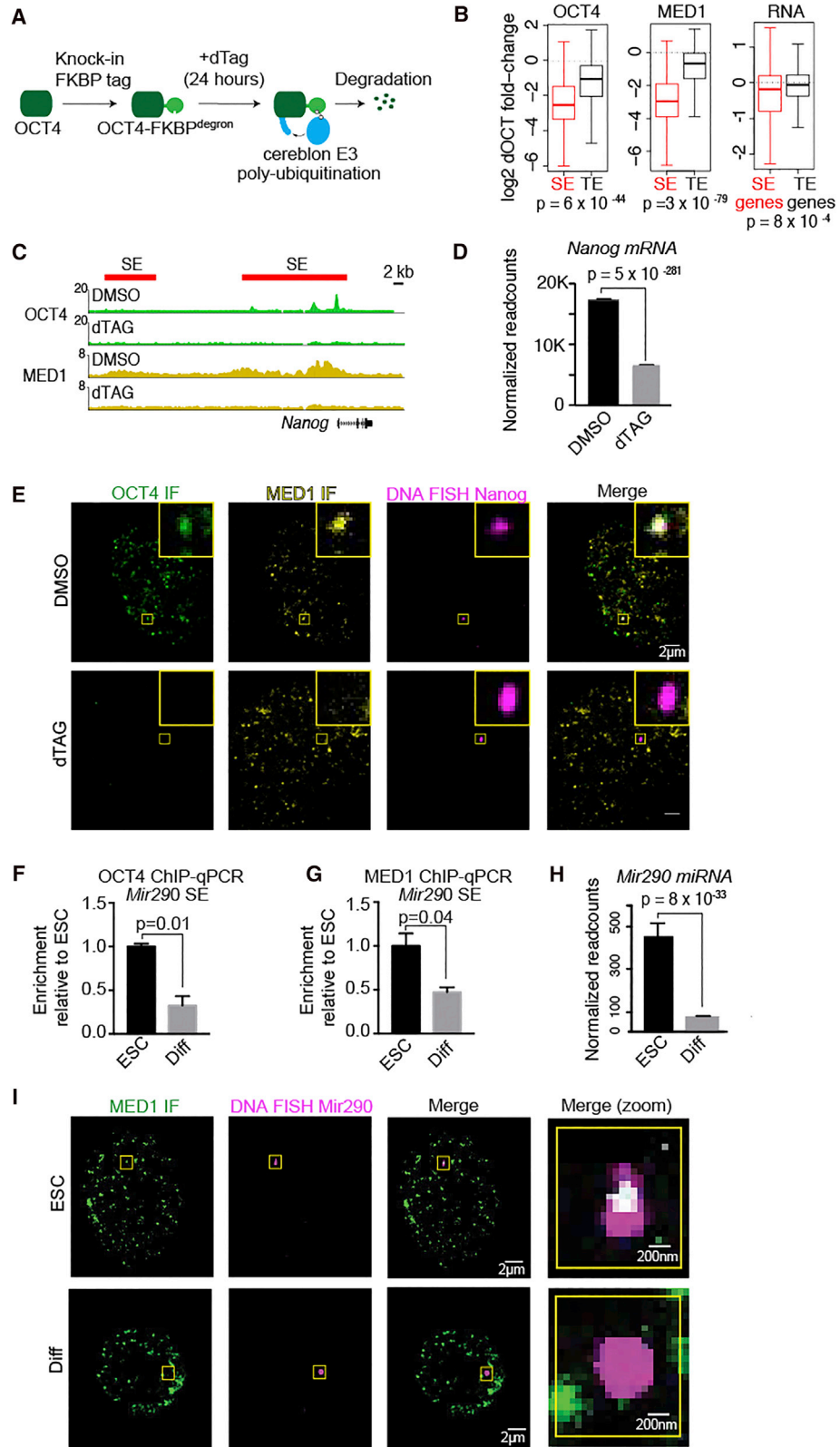
sensitive (Figures S3E and S3D). Thus, they exhibited characteristics associated with phase-separated liquid condensates (Barnani et al., 2017; Shin and Brangwynne, 2017). Furthermore, we found that OCT4-MED1-IDR droplets could form in the absence of any crowding agent (Figures S3E and S3F).

Residues Required for OCT4-MED1-IDR Droplet Formation and Gene Activation

We next investigated whether specific OCT4 amino acid residues are required for the formation of OCT4-MED1-IDR phase-separated droplets, as multiple categories of amino acid interaction have been implicated in forming condensates. For example, serine residues are required for MED1 phase separation (Sabari et al., 2018). We asked whether amino acid enrichments in the OCT4 ADs might point to a mechanism for interaction. An analysis of amino acid frequency and charge bias showed that the OCT4 IDRs are enriched in proline and glycine and have an overall acidic charge (Figure 4A). ADs are known to be enriched in acidic amino acids and proline and have historically been classified on this basis (Frieze and Farnham, 2011), but the mechanism by which these enrichments might cause gene activation

is not known. We hypothesized that proline or acidic amino acids in the ADs might facilitate interaction with the phase-separated MED1-IDR droplet. To test this, we designed fluorescently labeled proline and glutamic acid decapeptides and investigated whether these peptides can be concentrated in MED1-IDR droplets. When added to droplet formation buffer alone, these peptides remained in solution (Figure S4A). When mixed with MED1-IDR-GFP, however, proline peptides were not incorporated into MED1-IDR droplets, while the glutamic acid peptides were concentrated within (Figures 4B and S4B). These results show that peptides with acidic residues are amenable to incorporation within MED1 phase-separated droplets.

Based on these results, we deduced that an OCT4 protein lacking acidic amino acids in its ADs might be defective in its ability to phase separate with MED1-IDR. Such a dependence on acidic residues would be consistent with our observation that OCT4-MED1-IDR droplets are highly salt sensitive. To test this idea, we generated a mutant OCT4 in which all acidic residues in the ADs were replaced with alanine (thus changing 17 AAs in the N-terminal AD and 6 in the C-terminal AD) (Figure 4C). When this GFP-fused OCT4 mutant was mixed with purified



(legend on next page)

MED1-IDR, entry into droplets was highly attenuated (Figures 4C and S4C). To test whether this effect was specific for acidic residues, we generated a mutant of OCT4 in which all the aromatic amino acids within the ADs were changed to alanine. We found that this mutant was still incorporated into MED1-IDR droplets (Figures S4C and S4D). These results indicate that the ability of OCT4 to phase separate with MED1-IDR is dependent on acidic residues in the OCT4 IDRs.

To ensure that these results were not specific to the MED1-IDR, we explored whether purified Mediator complexes would form droplets *in vitro* and incorporate OCT4. The human Mediator complex was purified as previously described (Meyer et al., 2008) and then concentrated for use in the droplet formation assay (Figure S4E). Because purified endogenous Mediator does not contain a fluorescent tag, we monitored droplet formation by differential interference contrast (DIC) microscopy and found it to form droplets alone at ~200–400 nM (Figure 4D). Consistent with the results for MED1-IDR droplets, OCT4 was incorporated within human Mediator complex droplets, but incorporation of the OCT4 acidic mutant was attenuated. These results indicate that the MED1-IDR and the complete Mediator complex each exhibit phase-separating behaviors and suggest that they both incorporate OCT4 in a manner that is dependent on electrostatic interactions provided by acidic amino acids.

To test whether the OCT4 AD acidic mutations affect the ability of the factor to activate transcription *in vivo*, we utilized a GAL4 transactivation assay (Figure 4E). In this system, ADs or their mutant counterparts are fused to the GAL4 DBD and expressed in cells carrying a luciferase reporter plasmid. We found that the wild-type OCT4-AD fused to the GAL4-DBD was able to activate transcription, while the acidic mutant lost this function (Figure 4E). These results indicate that the acidic residues of the OCT4 ADs are necessary for both incorporation into MED1 phase-separated droplets *in vitro* and for gene activation *in vivo*.

Multiple TFs Phase Separate with Mediator Subunit Droplets

TFs with diverse types of ADs have been shown to interact with Mediator subunits, and MED1 is among the subunits that is

most targeted by TFs (Table S1). An analysis of mammalian TFs confirmed that TFs and their putative ADs are enriched in IDRs, as previous analyses have shown (Liu et al., 2006; Staby et al., 2017) (Figure 5A). We reasoned that many different TFs might interact with the MED1-IDR to generate liquid droplets and therefore be incorporated into MED1 condensates. To assess whether diverse MED1-interacting TFs can phase separate with MED1, we prepared purified recombinant, mEGFP-tagged, full-length MYC, p53, NANOG, SOX2, RAR α , GATA2, and ER (Table S3). When added to droplet formation buffers, most TFs formed droplets alone (Figure 5B). When added to droplet formation buffers with MED1-IDR, all 7 of these TFs concentrated into MED1-IDR droplets (Figures 5C and S5A). We selected p53 droplets for fluorescence recovery after photobleaching (FRAP) analysis; they exhibited rapid and dynamic internal reorganization (Figure S5B), supporting the notion that they are liquid condensates. These results indicate that TFs previously shown to interact with the MED1 subunit of Mediator can do so by forming phase-separated condensates with MED1.

Estrogen Stimulates Phase Separation of ER with MED1

ER is a well-studied example of a ligand-dependent TF. ER consists of an N-terminal ligand-independent AD, a central DBD, and a C-terminal ligand-dependent AD (also called the ligand binding domain [LBD]) (Figure 6A). Estrogen facilitates the interaction of ER with MED1 by binding the LBD of ER, which exposes a binding pocket for LXXLL motifs within the MED1-IDR (Figures 6A and 6B) (Manavathi et al., 2014). We noted that ER can form heterotypic droplets with the MED1-IDR recombinant protein used thus far in these studies (Figure 5C), which lacks the LXXLL motifs. This led us to investigate whether ER-MED1 droplet formation is responsive to estrogen and whether this involves the MED1 LXXLL motifs.

We performed droplet formation assays using a MED1-IDR recombinant protein containing LXXLL motifs (MED1-IDRXL-mCherry) and found that, similar to MED1-IDR and complete Mediator, it had the ability to form droplets alone (Figure 6C). We then tested the ability of ER to phase separate with MED1-IDRXL-mCherry and MED1-IDR-mCherry droplets.

Figure 2. MED1 Condensates Are Dependent on OCT4 Binding *In Vivo*

- (A) Schematic of OCT4 degradation. The C terminus of OCT4 is endogenously biallelically tagged with the FKBP protein; when exposed to the small molecule dTag, OCT4 is ubiquitinated and rapidly degraded.
- (B) Boxplot representation of log₂ fold change in OCT4 and MED1 ChIP-seq reads and RNA-seq reads of super-enhancer (SE)- or typical enhancer (TE)-driven genes, in ESCs carrying the OCT4 FKBP tag, treated with DMSO, or dTAG for 24 hr. The box represents the interquartile; whiskers are 1.5 \times the interquartile range.
- (C) Genome browser view of OCT4 (green) and MED1 (yellow) ChIP-seq data at the *Nanog* locus. The *Nanog* SE (red) shows a 90% reduction of OCT4 and MED1 binding after OCT4 degradation.
- (D) Normalized RNA-seq read counts of *Nanog* mRNA shows a 60% reduction upon OCT4 degradation. Error bars represent SEM.
- (E) Confocal microscopy images OCT4 and MED1 IF with DNA FISH to the *Nanog* locus in ESCs carrying the OCT4 FKBP tag, treated with DMSO or dTAG. Inset represents a zoomed in view of the yellow box. The merge view displays all three channels (OCT4 IF, MED1 IF, and *Nanog* DNA FISH) together.
- (F) OCT4 ChIP-qPCR to the *Mir290* SE in ESCs and differentiated cells (Diff) presented as enrichment over control, relative to signal in ESCs. Error bars represent the SEM from two biological replicates.
- (G) MED1 ChIP-qPCR to the *Mir290* SE in ESCs and differentiated cells (Diff) presented as enrichment over control, relative to signal in ESCs. Error bars represent the SEM from two biological replicates.
- (H) Normalized RNA-seq read counts of *Mir290* miRNA in ESCs or differentiated cells (Diff). Error bars represents the SEM from two biological replicates.
- (I) Confocal microscopy images of MED1 IF and DNA FISH to the *Mir290* genomic locus in ESCs and differentiated cells. Merge (zoom) represents a zoomed-in view of the yellow box in the merged channel.

See also Figure S2 and Tables S2 and S4.

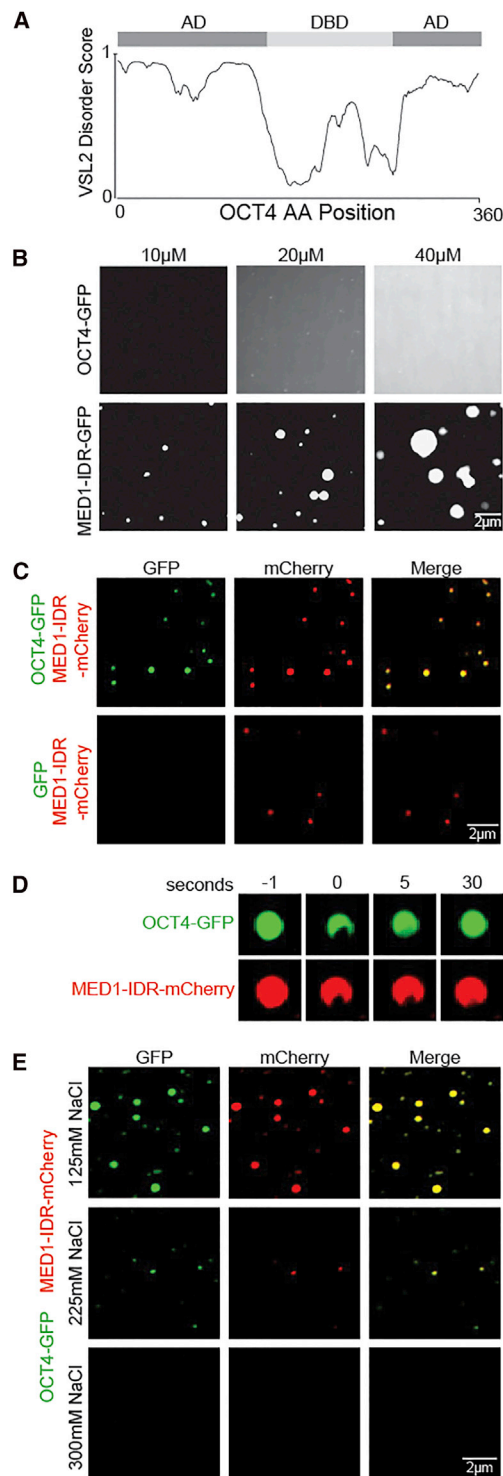


Figure 3. OCT4 Forms Liquid Droplets with MED1 *In Vitro*
 (A) Graph of intrinsic disorder of OCT4 as calculated by the VSL2 algorithm (<http://www.pondr.com/>). The DNA binding domain (DBD) and activation domains (ADs) are indicated above the disorder score graph (Brehm et al., 1997).
 (B) Representative images of droplet formation of OCT4-GFP (top row) and MED1-IDR-GFP (bottom row) at the indicated concentration in droplet formation buffer with 125 mM NaCl and 10% PEG-8000.
 (C) Representative images of droplet formation of MED1-IDR-mCherry mixed with GFP or OCT4-GFP at 10 μ M each in droplet formation buffer with 125 mM NaCl and 10% PEG-8000.
 (D) FRAP of heterotypic droplets of OCT4-GFP and MED1-IDR-mCherry. Confocal images were taken at indicated time points relative to photo-bleaching (0).
 (E) Representative images of droplet formation of 10 μ M MED1-IDR-mCherry and OCT4-GFP in droplet formation buffer with varying concentrations of salt and 10% PEG-8000.
 See also Figure S3 and Table S3.

Some recombinant ER was incorporated and concentrated into MED1-IDRXL-mCherry droplets, but the addition of estrogen considerably enhanced heterotypic droplet formation (Figures 6D and 6E). In contrast, the addition of estrogen had little effect on droplet formation when the experiment was conducted with MED1-IDR-mCherry, which lacks the LXXLL motifs (Figure S6). These results show that estrogen, which stimulates ER-mediated transcription *in vivo*, also stimulates incorporation of ER into MED1-IDR droplets *in vitro*. Thus, OCT4 and ER both require the same amino acids/ligands for both phase separation and activation. Furthermore, since the LBD is a structured domain that undergoes a conformation shift upon estrogen binding to interact with MED1, it appears that structured interactions may contribute to transcriptional condensate formation.

GCN4 and MED15 Phase Separation Is Dependent on Residues Required for Activation

Among the best-studied TF-coactivator systems is the yeast TF GCN4 and its interaction with the MED15 subunit of Mediator (Brzovic et al., 2011; Herbig et al., 2010; Jedidi et al., 2010). The GCN4 AD has been dissected genetically, the amino acids that contribute to activation have been identified (Drysdale et al., 1995; Staller et al., 2018), and recent studies have shown that the GCN4 AD interacts with MED15 in multiple orientations and conformations to form a “fuzzy complex” (Tuttle et al., 2018). Weak interactions that form fuzzy complexes have features of the IDR-IDR interactions that are thought to produce phase-separated condensates.

To test whether GCN4 and MED15 can form phase-separated droplets, we purified recombinant yeast GCN4-GFP and the N-terminal portion of yeast MED15-mCherry containing residues 6–651 (hereafter called MED15), which are responsible for the interaction with GCN4. When added separately to droplet formation buffer, GCN4 formed micrometer-sized droplets only at quite high concentrations (40 μ M), and MED15 formed only small droplets at this high concentration (Figure 7A). When mixed together, however, the GCN4 and MED15 recombinant proteins formed double-positive, micrometer-sized, spherical droplets at lower concentrations (Figures 7B and S7A). These GCN4-MED15 droplets exhibited rapid FRAP kinetics (Figure S7B), consistent with liquid-like behavior. We generated a phase diagram of these two proteins and found that they formed droplets together at low concentration (Figures S7C and S7D). This suggests that interaction between the two is required for phase separation at low concentration.

The ability of GCN4 to interact with MED15 and activate gene expression has been attributed to specific hydrophobic patches

and aromatic residues in the GCN4 AD (Drysdales et al., 1995; Staller et al., 2018; Tuttle et al., 2018). We created a mutant of GCN4 in which the 11 aromatic residues contained in these hydrophobic patches were changed to alanine (Figure 7C). When added to droplet formation buffers, the ability of the mutant protein to form droplets alone was attenuated (Figure S7E). Next, we tested whether droplet formation with MED15 was affected; indeed, the mutated protein has a compromised ability to form droplets with MED15 (Figures 7C and S7F). Similar results were obtained when GCN4 and the aromatic mutant of GCN4 was added to droplet formation buffers with the complete Mediator complex; while GCN4 was incorporated into Mediator droplets, the incorporation of the GCN4 mutant into Mediator droplets was attenuated (Figures 7D and S7G). These results demonstrate that multivalent, weak interactions between the AD of GCN4 and MED15 promote phase separation into liquid-like droplets.

The ADs of yeast TFs can function in mammalian cells and can do so by interacting with human Mediator (Oliviero et al., 1992). To investigate whether the aromatic mutant of GCN4 AD is impaired in its ability to recruit Mediator *in vivo*, the GCN4 AD and the GCN4 mutant AD were tethered to a Lac array in U2OS cells (Figure 7E) (Janicki et al., 2004). While the tethered GCN4 AD caused robust Mediator recruitment, the GCN4 aromatic mutant did not (Figure 7E). We used the GAL4 transactivation assay described previously to confirm that the GCN4 AD was capable of transcriptional activation *in vivo*, whereas the GCN4 aromatic mutant had lost that property (Figure 7F). These results provide further support for the idea that TF AD amino acids that are essential for phase separation with Mediator are required for gene activation.

DISCUSSION

The results described here support a model whereby TFs interact with Mediator and activate genes by the capacity of their ADs to form phase-separated condensates with this coactivator. For both the mammalian ESC pluripotency TF OCT4 and the yeast TF GCN4, we found that the AD amino acids required for phase separation with Mediator condensates were also required for gene activation *in vivo*. For ER, we found that estrogen stimulates the formation of phase-separated ER-MED1 droplets. ADs and coactivators generally consist of low-complexity amino acid sequences that have been classified as IDRs, and IDR-IDR interactions have been implicated in facilitating the formation of phase-separated condensates. We propose that IDR-mediated phase separation with Mediator is a general mechanism by which TF ADs effect gene expression and provide evidence that this occurs *in vivo* at SEs. We suggest that the ability to phase separate with Mediator, which would employ the features of high valency and low-affinity characteristic of liquid-liquid

phase-separated condensates, operates alongside an ability of some TFs to form high-affinity interactions with Mediator (Figure 7G) (Taatjes, 2017).

The model that TF ADs function by forming phase-separated condensates with coactivators explains several observations that are difficult to reconcile with classical lock-and-key models of protein-protein interaction. The mammalian genome encodes many hundreds of TFs with diverse ADs that must interact with a small number of coactivators (Allen and Taatjes, 2015; Arany et al., 1995; Avantsaggiati et al., 1996; Dai and Markham, 2001; Eckner et al., 1996; Gelman et al., 1999; Green, 2005; Liu et al., 2009; Merika et al., 1998; Oliner et al., 1996; Yin and Wang, 2014; Yuan et al., 1996), and ADs that share little sequence homology are functionally interchangeable among TFs (Godowski et al., 1988; Hope and Struhl, 1986; Jin et al., 2016; Lech et al., 1988; Ransone et al., 1990; Sadowski et al., 1988; Struhl, 1988; Tora et al., 1989). The common feature of ADs—the possession of low-complexity IDRs—is also a feature that is pronounced in coactivators. The model of coactivator interaction and gene activation by phase-separated condensate formation thus more readily explains how many hundreds of mammalian TFs interact with these coactivators.

Previous studies have provided important insights that prompted us to investigate the possibility that TF ADs function by forming phase-separated condensates. TF ADs have been classified by their amino acid profile as acidic, proline rich, serine/threonine rich, glutamine rich, or by their hypothetical shape as acid blobs, negative noodles, or peptide lassos (Sigler, 1988). Many of these features have been described for IDRs that are capable of forming phase-separated condensates (Babu, 2016; Darling et al., 2018; Das et al., 2015; Dunker et al., 2015; Habchi et al., 2014; van der Lee et al., 2014; Oldfield and Dunker, 2014; Uversky, 2017; Wright and Dyson, 2015). Evidence that the GCN4 AD interacts with MED15 in multiple orientations and conformations to form a “fuzzy complex” (Tuttle et al., 2018) is consistent with the notion of dynamic low-affinity interactions characteristic of phase-separated condensates. Likewise, the low complexity domains of the FET (FUS/EWS/TAF15) RNA-binding proteins (Andersson et al., 2008) can form phase-separated hydrogels and interact with the RNA polymerase II C-terminal domain (CTD) in a CTD phosphorylation-dependent manner (Kwon et al., 2013); this may explain the mechanism by which RNA polymerase II is recruited to active genes in its unphosphorylated state and released for elongation following phosphorylation of the CTD.

The model we describe here for TF AD function may explain the function of a class of heretofore poorly understood fusion oncoproteins. Many malignancies bear fusion-protein translocations involving portions of TFs (Bradner et al., 2017; Kim et al., 2017; Latysheva et al., 2016). These abnormal gene

Bottom: enrichment ratio of GFP, OCT4-GFP, or OCT4-acidic mutant-GFP in Mediator complex droplets. $n > 20$; error bars represent the distribution between the 10th and 90th percentiles.

(E) Top: GAL4 activation assay schematic. The GAL4 luciferase reporter plasmid was transfected into mouse ESCs with an expression vector for the GAL4-DBD fusion protein. Bottom: the AD activity was measured by luciferase activity of mouse ESCs transfected with GAL4-DBD, GAL4-OCT4-CAD, or GAL4-OCT4-CAD-acidic mutant. Error bars represent SEM.

See also Figure S4 and Table S3.

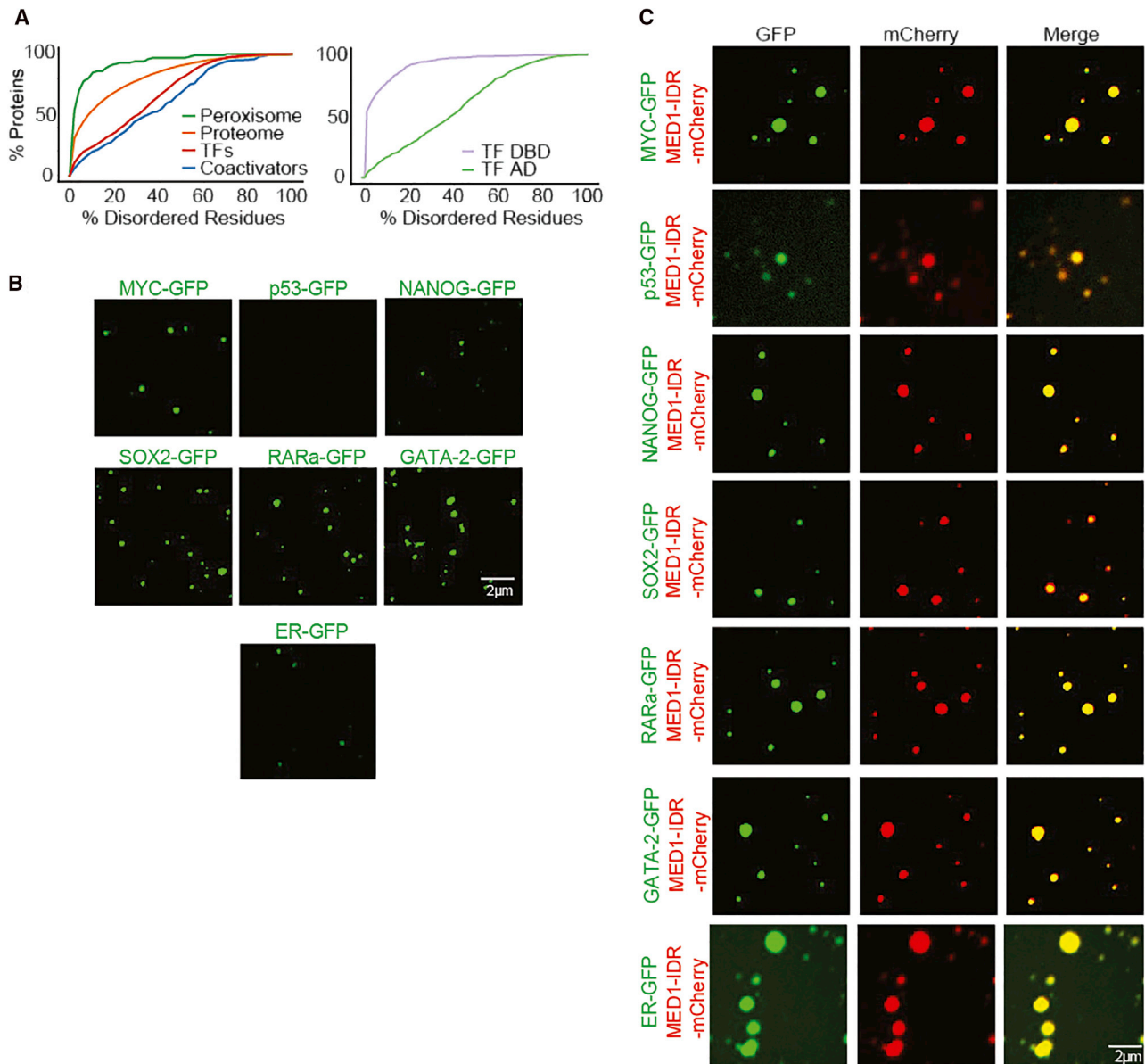


Figure 5. Multiple TFs Phase Separate with Mediator Droplets

(A) Left: percentage of disorder of various protein classes (x axis) plotted against the cumulative fraction of disordered proteins of that class (y axis). Right: disorder content of transcription factor (TF) DNA-binding domains (DBD) and putative activation domains (ADs).

(B) Representative images of droplet formation assaying homotypic droplet formation of indicated TFs. Recombinant MYC-GFP (12 µM), p53-GFP (40 µM), NANOG-GFP (10 µM), SOX2-GFP (40 µM), RARa-GFP (40 µM), GATA-2-GFP (40 µM), and ER-GFP (40 µM) was added to droplet formation buffers with 125 mM NaCl and 10% PEG-8000.

(C) Representative images of droplet formation showing that all tested TFs were incorporated into MED1-IDR droplets. 10 µM of MED1-IDRmCherry and 10 µM of MYC-GFP, p53-GFP, NANOG-GFP, SOX2-GFP, RARa-GFP, GATA-2-GFP, or ER-GFP were added to droplet formation buffers with 125 mM NaCl and 10% PEG-8000.

See also [Figure S5](#) and [Table S3](#).

products often fuse a DNA- or chromatin-binding domain to a wide array of partners, many of which are IDRs. For example, MLL may be fused to 80 different partner genes in AML ([Winters and Bernt, 2017](#)), the EWS-FLI rearrangement in Ewing's sarcoma causes malignant transformation by recruitment of a

disordered domain to oncogenes ([Boulay et al., 2017](#); [Chong et al., 2017](#)), and the disordered phase-separating protein FUS is found fused to a DBD in certain sarcomas ([Croizat et al., 1993](#); [Patel et al., 2015](#)). Phase separation provides a mechanism by which such gene products result in aberrant

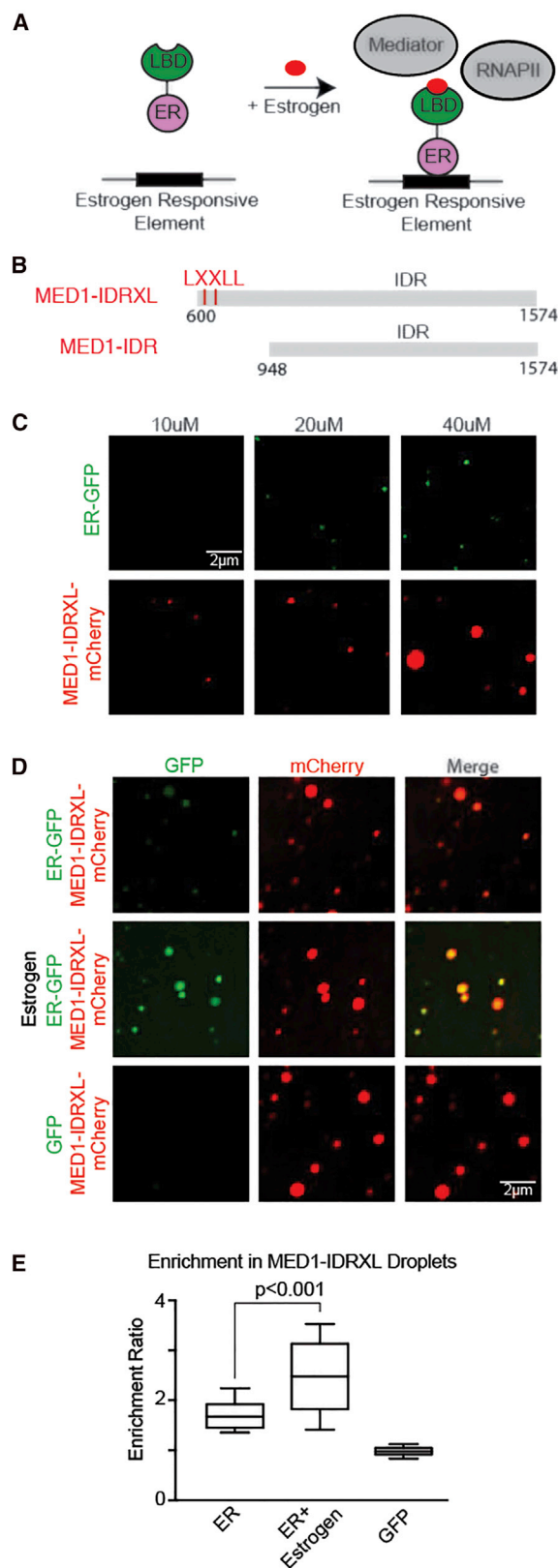


Figure 6. Estrogen Stimulates Phase Separation of ER with MED1

(A) Schematic of estrogen stimulated gene activation. Estrogen facilitates the interaction of ER with Mediator and RNAPII by binding the ligand binding domain (LBD) of ER, which exposes a binding pocket for LXXLL motifs within the MED1-IDR.

(B) Schematic view of MED1-IDRXL and MED1-IDR used for recombinant protein production.

(C) Representative images of droplet formation, assaying homotypic droplet formation of ER-GFP, and MED1-IDRXL-mCherry performed with the indicated protein concentration in droplet formation buffers with 125 mM NaCl and 10% PEG-8000.

(D) Representative confocal images of droplet formation showing that ER is incorporated into MED1-IDRXL droplets and the addition of estrogen enhanced heterotypic droplet formation. ER-GFP, ER-GFP in the presence of estrogen, or GFP is mixed with MED1-IDRXL. 10 μ M of each indicated protein was added to droplet formation buffers with 125 mM NaCl and 10% PEG-8000.

(E) Enrichment ratio in MED1-IDRXL droplets of ER-GFP, ER-GFP in the presence of estrogen, or GFP. $n > 20$; error bars represent the distribution between the 10th and 90th percentiles.

See also [Figure S6](#) and [Table S3](#).

gene expression programs; by recruiting a disordered protein to the chromatin, diverse coactivators may form phase-separated condensates to drive oncogene expression. Understanding the interactions that compose these aberrant transcriptional condensates, their structures, and behaviors may open new therapeutic avenues.

STAR METHODS

Detailed methods are provided in the online version of this paper and include the following:

- [KEY RESOURCES TABLE](#)
- [CONTACT FOR REAGENT AND RESOURCE SHARING](#)
- [EXPERIMENTAL MODEL AND SUBJECT DETAILS](#)
 - Cells
 - Cell culture conditions
- [METHOD DETAILS](#)
 - Immunofluorescence with RNA FISH
 - Immunofluorescence with DNA FISH
 - Tissue culture
 - Western blot
 - Chromatin immunoprecipitation (ChIP) qPCR and sequencing
 - RNA-Seq
 - Protein purification
 - *In vitro* droplet assay
 - Genome editing and protein degradation
 - GAL4 transcription assay
 - Lac binding assay
 - Purification of CDK8-Mediator
- [QUANTIFICATION AND STATISTICAL ANALYSIS](#)
 - Experimental design
 - Average image and radial distribution analysis
 - Chromatin immunoprecipitation PCR and sequencing (ChIP) analysis
 - Super-enhancer identification
 - RNA-Seq analysis
 - Enrichment and charge analysis of OCT4

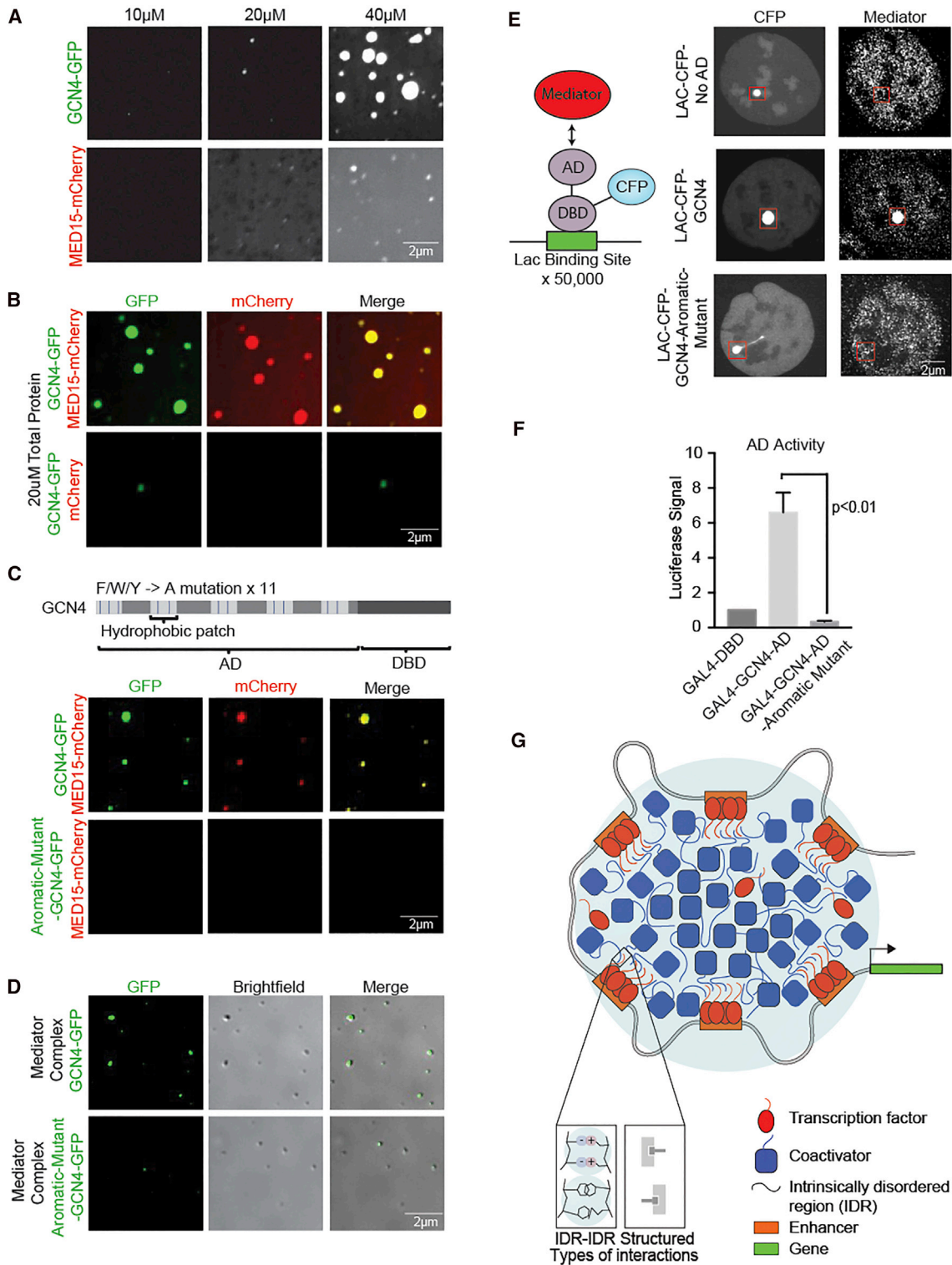


Figure 7. TF-Coactivator Phase Separation Is Dependent on Residues Required for Transactivation

(A) Representative confocal images of droplet formation of GCN4-GFP or MED15-mCherry were added to droplet formation buffers with 125 mM NaCl and 10% PEG-8000.

(B) Representative images of droplet formation showing that GCN4 forms droplets with MED15. GCN4-GFP and mCherry or GCN4-GFP and MED15-mCherry were added to droplet formation buffers at 10 μ M with 125 mM NaCl and 10% PEG-8000 and imaged on a fluorescent microscope with the indicated filters.

(legend continued on next page)

- Disorder enrichment analysis
- Imaging analysis of *in vitro* droplets
- **DATA AND SOFTWARE AVAILABILITY**
- Datasets

SUPPLEMENTAL INFORMATION

Supplemental Information includes seven figures and four tables and can be found with this article online at <https://doi.org/10.1016/j.cell.2018.10.042>.

ACKNOWLEDGMENTS

We thank Wendy Salmon of the W.M. Keck Microscopy Facility, the Whitehead Genomics Core, Arup Chakraborty, and Philip A. Sharp. The work was supported by NIH grant GM123511 and NSF grant PHY1743900 (R.A.Y.), NIH grant GM117370 (D.J.T.), Swedish Research Council Postdoctoral Fellowship (VR 2017-00372) (A.B.), NIH grant T32CA009172 (I.A.K.), a Damon Runyon Cancer Research Foundation Fellowship (2309-17) (B.R.S.), a NSF Graduate Research Fellowship (A.V.Z.), a Hope Funds for Cancer Research fellowship (B.J.A.), a Cancer Research Institute Irvington Fellowship (Y.E.G.), NIH grant T32GM08759 (C.B.F.), and a NWO Rubicon Fellowship (J.S.).

AUTHOR CONTRIBUTIONS

Conceptualization, A.B., I.A.K., and R.A.Y.; Methodology, A.B., I.A.K., B.R.S., A.D., and E.L.C.; Software, K.S. and B.J.A.; Formal Analysis, A.B., I.A.K., C.H.L., K.S., and B.J.A.; Investigation, A.B., I.A.K., B.R.S., A.D., E.L.C., A.V.Z., C.H.L., J.C.M., N.M.H., L.K.A., Y.E.G., J.K.R., C.B.F., and J.S.; Resources, D.J.T. and R.A.Y.; Data Curation, B.J.A.; Writing – Original Draft, A.B., I.A.K., and R.A.Y.; Writing – Reviewing and Editing, all authors; Visualization, A.B., I.A.K., B.R.S., A.D., C.H.L., K.S., B.J.A., and J.S.; Supervision, T.I.L., D.J.T., and R.A.Y.; Project Administration, A.B., I.A.K., and R.A.Y.; Funding Acquisition, D.J.T. and R.A.Y.

DECLARATION OF INTERESTS

The Whitehead Institute filed a patent application based in part on this paper. R.A.Y. is a founder and shareholder of Syros Pharmaceuticals, Camp4 Therapeutics, and Omega Therapeutics. I.A.K. is a consultant to InfiniteMD, Best Doctors, and Foundation Medicine and is a shareholder of InfiniteMD. B.J.A. and T.I.L. are shareholders of Syros Pharmaceuticals. T.I.L. is a consultant to Camp4 Therapeutics.

Received: June 12, 2018

Revised: August 20, 2018

Accepted: October 16, 2018

Published: November 15, 2018

REFERENCES

- Alberti, S. (2017). The wisdom of crowds: Regulating cell function through condensed states of living matter. *J. Cell Sci.* *130*, 2789–2796.
- Allen, B.L., and Taatjes, D.J. (2015). The Mediator complex: A central integrator of transcription. *Nat. Rev. Mol. Cell Biol.* *16*, 155–166.
- Andersson, M.K., Ståhlberg, A., Arvidsson, Y., Olofsson, A., Semb, H., Stenman, G., Nilsson, O., and Åman, P. (2008). The multifunctional FUS, EWS and TAF15 proto-oncoproteins show cell type-specific expression patterns and involvement in cell spreading and stress response. *BMC Cell Biol.* *9*, 37.
- Apostolou, E., Ferrari, F., Walsh, R.M., Bar-Nur, O., Stadtfeld, M., Cheloufi, S., Stuart, H.T., Polo, J.M., Ohsumi, T.K., Borowsky, M.L., et al. (2013). Genome-wide chromatin interactions of the Nanog locus in pluripotency, differentiation, and reprogramming. *Cell Stem Cell* *12*, 699–712.
- Arany, Z., Newsome, D., Oldread, E., Livingston, D.M., and Eckner, R. (1995). A family of transcriptional adaptor proteins targeted by the E1A oncoprotein. *Nature* *374*, 81–84.
- Avantaggiati, M.L., Carbone, M., Graessmann, A., Nakatani, Y., Howard, B., and Levine, A.S. (1996). The SV40 large T antigen and adenovirus E1a oncoproteins interact with distinct isoforms of the transcriptional co-activator, p300. *EMBO J.* *15*, 2236–2248.
- Babu, M.M. (2016). The contribution of intrinsically disordered regions to protein function, cellular complexity, and human disease. *Biochem. Soc. Trans.* *44*, 1185–1200.
- Banani, S.F., Lee, H.O., Hyman, A.A., and Rosen, M.K. (2017). Biomolecular condensates: Organizers of cellular biochemistry. *Nat. Rev. Mol. Cell Biol.* *18*, 285–298.
- Boulay, G., Sandoval, G.J., Riggi, N., Iyer, S., Buisson, R., Naigles, B., Awad, M.E., Rengarajan, S., Volorio, A., McBride, M.J., et al. (2017). Cancer-specific retargeting of BAF complexes by a prion-like domain. *Cell* *171*, 163–178.
- Bradner, J.E., Hnisz, D., and Young, R.A. (2017). Transcriptional addiction in cancer. *Cell* *9*, 629–643.
- Brehm, A., Ohbo, K., and Schöler, H. (1997). The carboxy-terminal transactivation domain of Oct-4 acquires cell specificity through the POU domain. *Mol. Cell Biol.* *17*, 154–162.
- Brent, R., and Ptashne, M. (1985). A eukaryotic transcriptional activator bearing the DNA specificity of a prokaryotic repressor. *Cell* *43*, 729–736.
- Brzovic, P.S., Heikaus, C.C., Kisselev, L., Vernon, R., Herbig, E., Pacheco, D., Warfield, L., Littlefield, P., Baker, D., Klevit, R.E., and Hahn, S. (2011). The acidic transcription activator Gcn4 binds the mediator subunit Gal11/Med15 using a simple protein interface forming a fuzzy complex. *Mol. Cell* *44*, 942–953.
- Burke, K.A., Janke, A.M., Rhine, C.L., and Fawzi, N.L. (2015). Residue-by-residue view of *in vitro* FUS granules that bind the C-terminal domain of RNA polymerase II. *Mol. Cell* *60*, 231–241.

(C) Top: schematic of GCN4 protein composed of an activation domain (AD) and DNA-binding domain (DBD). Aromatic residues in the hydrophobic patches of the AD are marked by blue lines. All 11 aromatic residues in the hydrophobic patches were mutated to alanine to generate a GCN4-aromatic mutant. Bottom: representative images of droplet formation showing that the ability of GCN4 aromatic mutant to form droplets with MED15 is attenuated. GCN4-GFP or GCN4-Aromatic mutant-GFP and MED15-mCherry were added to droplet formation at 10 μ M each with 125 mM NaCl and 10% PEG-8000.

(D) Representative images of droplet formation showing that GCN4 wild-type but not GCN4 aromatic mutant are incorporated into Mediator complex droplets. 10 μ M of GCN4-GFP or GCN4-Aromatic mutant-GFP was mixed with purified Mediator complex in droplet formation buffer with 125 mM NaCl and 10% PEG-8000.

(E) Left: schematic of the Lac assay. A U2OS cell bearing 50,000 repeats of the Lac operon is transfected with a Lac binding domain-CFP-AD fusion protein. Right: IF of MED1 in Lac-U2OS cells transfected with the indicated Lac binding protein construct.

(F) GAL4 activation assay. Transcriptional output as measured by luciferase activity in 293T cells, of the indicated activation domain fused to the GAL4 DBD. Error bars represent SEM.

(G) Model showing TFs and coactivators forming phase-separated condensates at SEs to drive gene activation. In this model, transcriptional condensates incorporate both dynamic and structured interactions.

See also [Figure S7](#) and [Table S3](#).

- Chong, S., Dugast-darzacq, C., Liu, Z., Dong, P., and Dailey, G.M. (2017). Dynamic and selective low-complexity domain interactions revealed by live-cell single-molecule imaging. *bioRxiv*. <https://doi.org/10.1101/208710>.
- Crozat, A., Åman, P., Mandahl, N., and Ron, D. (1993). Fusion of CHOP to a novel RNA-binding protein in human myxoid liposarcoma. *Nature* **363**, 640–644.
- Dai, Y.S., and Markham, B.E. (2001). p300 Functions as a coactivator of transcription factor GATA-4. *J. Biol. Chem.* **276**, 37178–37185.
- Darling, A.L., Liu, Y., Oldfield, C.J., and Uversky, V.N. (2018). Intrinsically disordered proteome of human membrane-less organelles. *Proteomics* **18**, e1700193.
- Das, R.K., Ruff, K.M., and Pappu, R.V. (2015). Relating sequence encoded information to form and function of intrinsically disordered proteins. *Curr. Opin. Struct. Biol.* **32**, 102–112.
- Drysdale, C.M., Dueñas, E., Jackson, B.M., Reusser, U., Braus, G.H., and Hinnebusch, A.G. (1995). The transcriptional activator GCN4 contains multiple activation domains that are critically dependent on hydrophobic amino acids. *Mol. Cell. Biol.* **15**, 1220–1233.
- Dunker, A.K., Bondos, S.E., Huang, F., and Oldfield, C.J. (2015). Intrinsically disordered proteins and multicellular organisms. *Semin. Cell Dev. Biol.* **37**, 44–55.
- Eckner, R., Yao, T.P., Oldread, E., and Livingston, D.M. (1996). Interaction and functional collaboration of p300/CBP and bHLH proteins in muscle and B-cell differentiation. *Genes Dev.* **10**, 2478–2490.
- Frietze, S., and Farnham, P.J. (2011). Transcription factor effector domains. *Subcell. Biochem.* **52**, 261–277.
- Fulton, D.L., Sundararajan, S., Badis, G., Hughes, T.R., Wasserman, W.W., Roach, J.C., and Sladek, R. (2009). TFCat: The curated catalog of mouse and human transcription factors. *Genome Biol.* **10**, R29.
- Gelman, L., Zhou, G., Fajas, L., Raspé, E., Fruchart, J.C., and Auwerx, J. (1999). p300 interacts with the N- and C-terminal part of PPAR γ 2 in a ligand-independent and -dependent manner, respectively. *J. Biol. Chem.* **274**, 7681–7688.
- Godowski, P.J., Picard, D., and Yamamoto, K.R. (1988). Signal transduction and transcriptional regulation by glucocorticoid receptor-LexA fusion proteins. *Science* **241**, 812–816.
- Green, M.R. (2005). Eukaryotic transcription activation: Right on target. *Mol. Cell* **18**, 399–402.
- Habchi, J., Tompa, P., Longhi, S., and Uversky, V.N. (2014). Introducing protein intrinsic disorder. *Chem. Rev.* **114**, 6561–6588.
- Herbig, E., Warfield, L., Fish, L., Fishburn, J., Knutson, B.A., Moorefield, B., Pacheco, D., and Hahn, S. (2010). Mechanism of Mediator recruitment by tandem Gcn4 activation domains and three Gal11 activator-binding domains. *Mol. Cell. Biol.* **30**, 2376–2390.
- Hnisz, D., Shrinivas, K., Young, R.A., Chakraborty, A.K., and Sharp, P.A. (2017). A phase separation model for transcriptional control. *Cell* **169**, 13–23.
- Holehouse, A.S., Das, R.K., Ahad, J.N., Richardson, M.O.G., and Pappu, R.V. (2017). CIDER: Resources to analyze sequence-ensemble relationships of intrinsically disordered proteins. *Biophys. J.* **112**, 16–21.
- Hope, I.A., and Struhl, K. (1986). Functional dissection of a eukaryotic transcriptional activator protein, GCN4 of yeast. *Cell* **46**, 885–894.
- Hume, M.A., Barrera, L.A., Gisselbrecht, S.S., and Bulyk, M.L. (2015). UniPROBE, update 2015: New tools and content for the online database of protein-binding microarray data on protein-DNA interactions. *Nucleic Acids Res.* **43**, D117–D122.
- Hyman, A.A., Weber, C.A., and Jülicher, F. (2014). Liquid-liquid phase separation in biology. *Annu. Rev. Cell Dev. Biol.* **30**, 39–58.
- Janicki, S.M., Tsukamoto, T., Salghetti, S.E., Tansey, W.P., Sachidanandam, R., Prasanth, K.V., Ried, T., Shav-Tal, Y., Bertrand, E., Singer, R.H., and Spector, D.L. (2004). From silencing to gene expression: Real-time analysis in single cells. *Cell* **116**, 683–698.
- Jedidi, I., Zhang, F., Qiu, H., Stahl, S.J., Palmer, I., Kaufman, J.D., Nadaud, P.S., Mukherjee, S., Wingfield, P.T., Jaroniec, C.P., and Hinnebusch, A.G. (2010). Activator Gcn4 employs multiple segments of Med15/Gal11, including the KIX domain, to recruit mediator to target genes in vivo. *J. Biol. Chem.* **285**, 2438–2455.
- Jin, W., Wang, L., Zhu, F., Tan, W., Lin, W., Chen, D., Sun, Q., and Xia, Z. (2016). Critical POU domain residues confer Oct4 uniqueness in somatic cell reprogramming. *Sci. Rep.* **6**, 20818.
- Jolma, A., Yan, J., Whittington, T., Toivonen, J., Nitta, K.R., Rastas, P., Morgunova, E., Enge, M., Taipale, M., Wei, G., et al. (2013). DNA-binding specificities of human transcription factors. *Cell* **152**, 327–339.
- Juven-Gershon, T., and Kadonaga, J.T. (2010). Regulation of gene expression via the core promoter and the basal transcriptional machinery. *Dev. Biol.* **339**, 225–229.
- Keegan, L., Gill, G., and Ptashne, M. (1986). Separation of DNA binding from the transcription-activating function of a eukaryotic regulatory protein. *Science* **231**, 699–704.
- Khan, A., Fomes, O., Stigliani, A., Gheorghe, M., Castro-Mondragon, J.A., van der Lee, R., Bessy, A., Chêneby, J., Kulkarni, S.R., Tan, G., et al. (2018). JASPAR 2018: Update of the open-access database of transcription factor binding profiles and its web framework. *Nucleic Acids Res.* **46** (D1), D260–D266.
- Kim, P., Ballester, L.Y., and Zhao, Z. (2017). Domain retention in transcription factor fusion genes and its biological and clinical implications: A pan-cancer study. *Oncotarget* **8**, 110103–110117.
- Kwon, I., Kato, M., Xiang, S., Wu, L., Theodoropoulos, P., Mirzaei, H., Han, T., Xie, S., Corden, J.L., and McKnight, S.L. (2013). Phosphorylation-Regulated Binding of RNA Polymerase II to Fibrous Polymers of Low-Complexity Domains. *Cell* **155**, 1049–1060.
- Latysheva, N.S., Oates, M.E., Maddox, L., Flock, T., Gough, J., Buljan, M., Weatheritt, R.J., and Babu, M.M. (2016). Molecular principles of gene fusion mediated rewiring of protein interaction networks in cancer. *Mol. Cell* **63**, 579–592.
- Lech, K., Anderson, K., and Brent, R. (1988). DNA-bound Fos proteins activate transcription in yeast. *Cell* **52**, 179–184.
- Lin, Y., Protter, D.S.W., Rosen, M.K., and Parker, R. (2015). Formation and maturation of phase-separated liquid droplets by RNA-binding proteins. *Mol. Cell* **60**, 208–219.
- Liu, J., Perumal, N.B., Oldfield, C.J., Su, E.W., Uversky, V.N., and Dunker, A.K. (2006). Intrinsic disorder in transcription factors. *Biochemistry* **45**, 6873–6888.
- Liu, W.-L., Coleman, R.A., Ma, E., Grob, P., Yang, J.L., Zhang, Y., Dailey, G., Nogales, E., and Tjian, R. (2009). Structures of three distinct activator-TFIID complexes. *Genes Dev.* **23**, 1510–1521.
- Malik, S., and Roeder, R.G. (2010). The metazoan Mediator co-activator complex as an integrative hub for transcriptional regulation. *Nat. Rev. Genet.* **11**, 761–772.
- Manavathi, B., Samanthapudi, V.S.K., and Gajulapalli, V.N.R. (2014). Estrogen receptor coregulators and pioneer factors: The orchestrators of mammary gland cell fate and development. *Front. Cell Dev. Biol.* **2**, 34.
- Merika, M., Williams, A.J., Chen, G., Collins, T., and Thanos, D. (1998). Recruitment of CBP/p300 by the IFN β enhanceosome is required for synergistic activation of transcription. *Mol. Cell* **1**, 277–287.
- Meyer, K.D., Donner, A.J., Knuesel, M.T., York, A.G., Espinosa, J.M., and Taatjes, D.J. (2008). Cooperative activity of cdk8 and GCN5L within Mediator directs tandem phosphoacetylation of histone H3. *EMBO J.* **27**, 1447–1457.
- Mitchell, P.J., and Tjian, R. (1989). Transcriptional regulation in mammalian cells by sequence-specific DNA binding proteins. *Science* **245**, 371–378.
- Nabet, B., Roberts, J.M., Buckley, D.L., Paulk, J., Dastjerdi, S., Yang, A., Leggett, A.L., Erb, M.A., Lawlor, M.A., Souza, A., et al. (2018). The dTAG system for immediate and target-specific protein degradation. *Nat. Chem. Biol.* **14**, 431–441.
- Nott, T.J., Petsalaki, E., Farber, P., Jervis, D., Fussner, E., Plochowietz, A., Craggs, T.D., Bazett-Jones, D.P., Pawson, T., Forman-Kay, J.D., and Baldwin,

- A.J. (2015). Phase transition of a disordered nuage protein generates environmentally responsive membraneless organelles. *Mol. Cell* 57, 936–947.
- Oates, M.E., Romero, P., Ishida, T., Ghalwash, M., Mizianty, M.J., Xue, B., Dosztányi, Z., Uversky, V.N., Obradovic, Z., Kurgan, L., et al. (2013). D²P²: Database of disordered protein predictions. *Nucleic Acids Res.* 41, D508–D516.
- Oldfield, C.J., and Dunker, A.K. (2014). Intrinsically disordered proteins and intrinsically disordered protein regions. *Annu. Rev. Biochem.* 83, 553–584.
- Oliner, J.D., Andresen, J.M., Hansen, S.K., Zhou, S., and Tjian, R. (1996). SREBP transcriptional activity is mediated through an interaction with the CREB-binding protein. *Genes Dev.* 10, 2903–2911.
- Oliviero, S., Robinson, G.S., Struhl, K., and Spiegelman, B.M. (1992). Yeast GCN4 as a probe for oncogenesis by AP-1 transcription factors: Transcriptional activation through AP-1 sites is not sufficient for cellular transformation. *Genes Dev.* 6, 1799–1809.
- Panne, D., Maniatis, T., and Harrison, S.C. (2007). An atomic model of the interferon- β enhanceosome. *Cell* 129, 1111–1123.
- Patel, A., Lee, H.O., Jawerth, L., Maharana, S., Jahnel, M., Hein, M.Y., Stoynov, S., Mahamid, J., Saha, S., Franzmann, T.M., et al. (2015). A liquid-to-solid phase transition of the ALS protein FUS accelerated by disease mutation. *Cell* 162, 1066–1077.
- Plaschka, C., Nozawa, K., and Cramer, P. (2016). Mediator architecture and RNA polymerase II interaction. *J. Mol. Biol.* 428, 2569–2574.
- Ransone, L.J., Wamsley, P., Morley, K.L., and Verma, I.M. (1990). Domain swapping reveals the modular nature of Fos, Jun, and CREB proteins. *Mol. Cell Biol.* 10, 4565–4573.
- Reiter, F., Wienerroither, S., and Stark, A. (2017). Combinatorial function of transcription factors and cofactors. *Curr. Opin. Genet. Dev.* 43, 73–81.
- Roberts, S.G. (2000). Mechanisms of action of transcription activation and repression domains. *Cell. Mol. Life Sci.* 57, 1149–1160.
- Sabari, B.R., Dall’Agnese, A., Boija, A., Klein, I.A., Coffey, E.L., Shrinivas, K., Abraham, B.J., Hannett, N.M., Zamudio, A.V., Manteiga, J.C., et al. (2018). Coactivator condensation at super-enhancers links phase separation and gene control. *Science* 361, 80.
- Sadowski, I., Ma, J., Triezenberg, S., and Ptashne, M. (1988). GAL4-VP16 is an unusually potent transcriptional activator. *Nature* 335, 563–564.
- Saint-andré, V., Federation, A.J., Lin, C.Y., Abraham, B.J., Reddy, J., Lee, T.I., Bradner, J.E., and Young, R.A. (2016). Models of human core transcriptional regulatory circuitries. *Genome Res.* 26, 385–396.
- Schindelin, J., Arganda-Carreras, I., Frise, E., Kaynig, V., Longair, M., Pietzsch, T., Preibisch, S., Rueden, C., Saalfeld, S., Schmid, B., et al. (2012). Fiji: an open-source platform for biological-image analysis. *Nat. Methods* 9, 676–682.
- Shin, Y., and Brangwynne, C.P. (2017). Liquid phase condensation in cell physiology and disease. *Science*. Published online September 22, 2017. <https://doi.org/10.1126/science.aaf4382>.
- Sigler, P.B. (1988). Transcriptional activation. Acid blobs and negative nodules. *Nature* 333, 210–212.
- Soutourina, J. (2018). Transcription regulation by the Mediator complex. *Nat. Rev. Mol. Cell Biol.* 19, 262–274.
- Staby, L., O’Shea, C., Willemoës, M., Theisen, F., Kragelund, B.B., and Skriver, K. (2017). Eukaryotic transcription factors: Paradigms of protein intrinsic disorder. *Biochem. J.* 474, 2509–2532.
- Staller, M.V., Holehouse, A.S., Swain-Lenz, D., Das, R.K., Pappu, R.V., and Cohen, B.A. (2018). A high-throughput mutational scan of an intrinsically disordered acidic transcriptional activation domain. *Cell Syst.* 6, 444–455.
- Struhl, K. (1988). The JUN oncoprotein, a vertebrate transcription factor, activates transcription in yeast. *Nature* 332, 649–650.
- Taatjes, D.J. (2010). The human Mediator complex: A versatile, genome-wide regulator of transcription. *Trends Biochem. Sci.* 35, 315–322.
- Taatjes, D.J. (2017). Transcription factor-mediator interfaces: Multiple and multi-valent. *J. Mol. Biol.* 429, 2996–2998.
- Tompa, P., and Fuxreiter, M. (2008). Fuzzy complexes: Polymorphism and structural disorder in protein-protein interactions. *Trends Biochem. Sci.* 33, 2–8.
- Tora, L., White, J., Brou, C., Tasset, D., Webster, N., Scheer, E., and Chambon, P. (1989). The human estrogen receptor has two independent nonacidic transcriptional activation functions. *Cell* 59, 477–487.
- Triezenberg, S.J. (1995). Structure and function of transcriptional activation domains. *Curr. Opin. Genet. Dev.* 5, 190–196.
- Tuttle, L.M., Pacheco, D., Warfield, L., Luo, J., Ranish, J., Hahn, S., and Klevit, R.E. (2018). Gcn4-mediator specificity is mediated by a large and dynamic fuzzy protein-protein complex. *Cell Rep.* 22, 3251–3264.
- Uversky, V.N. (2017). Intrinsically disordered proteins in overcrowded milieu: Membrane-less organelles, phase separation, and intrinsic disorder. *Curr. Opin. Struct. Biol.* 44, 18–30.
- van der Lee, R., Buljan, M., Lang, B., Weatheritt, R.J., Daughdrill, G.W., Dunker, A.K., Fuxreiter, M., Gough, J., Gsponer, J., Jones, D.T., et al. (2014). Classification of intrinsically disordered regions and proteins. *Chem. Rev.* 114, 6589–6631.
- Vaquerezas, J.M., Kummerfeld, S.K., Teichmann, S.A., and Luscombe, N.M. (2009). A census of human transcription factors: Function, expression and evolution. *Nat. Rev. Genet.* 10, 252–263.
- Warfield, L., Tuttle, L.M., Pacheco, D., Klevit, R.E., and Hahn, S. (2014). A sequence-specific transcription activator motif and powerful synthetic variants that bind Mediator using a fuzzy protein interface. *Proc. Natl. Acad. Sci. USA* 111, E3506–E3513.
- Weintraub, A.S., Li, C.H., Zamudio, A.V., Sigova, A.A., Hannett, N.M., Day, D.S., Abraham, B.J., Cohen, M.A., Nabet, B., Buckley, D.L., et al. (2017). YY1 is a structural regulator of enhancer-promoter loops. *Cell* 171, 1573–1588.
- Wheeler, R.J., and Hyman, A.A. (2018). Controlling compartmentalization by non-membrane-bound organelles. *Philos. Trans. R. Soc. Lond. B Biol. Sci.* 26, 373.
- Whyte, W.A., Orlando, D.A., Hnisz, D., Abraham, B.J., Lin, C.Y., Kagey, M.H., Rahl, P.B., Lee, T.I., and Young, R.A. (2013). Master transcription factors and mediator establish super-enhancers at key cell identity genes. *Cell* 153, 307–319.
- Winters, A.C., and Bernt, K.M. (2017). MLL-rearranged leukemias—An update on science and clinical approaches. *Front Pediatr.* 5, 4.
- Wright, P.E., and Dyson, H.J. (2015). Intrinsically disordered proteins in cellular signalling and regulation. *Nat. Rev. Mol. Cell Biol.* 16, 18–29.
- Yin, J.W., and Wang, G. (2014). The Mediator complex: A master coordinator of transcription and cell lineage development. *Development* 141, 977–987.
- Yuan, W., Condorelli, G., Caruso, M., Felsani, A., and Giordano, A. (1996). Human p300 protein is a coactivator for the transcription factor MyoD. *J. Biol. Chem.* 271, 9009–9013.

STAR★METHODS

KEY RESOURCES TABLE

| REAGENT or RESOURCE | SOURCE | IDENTIFIER |
|--|------------------------------------|---------------------------------|
| Antibodies | | |
| MED1 | Abcam | ab64965 |
| OCT4 | Santa Cruz | sc-5279X |
| Goat anti-Rabbit IgG Alexa Fluor 488 | Life Technologies | A11008 |
| Goat anti-Rabbit IgG Alexa Fluor 568 | Life Technologies | A11011 |
| Goat anti-Mouse IgG Alexa Fluor 674 | Thermo Fisher | A21235 |
| Med1 | Bethyl | A300-793A-4 |
| Oct4 | Santa Cruz | sc-8628x |
| Beta-Actin | Santa Cruz | sc-7210 |
| HA | abcam | ab9110 |
| Bacterial and Virus Strains | | |
| LOBSTR cells | Cheeseman Lab (WI/MIT) | N/A |
| Chemicals, Peptides, and Recombinant Proteins | | |
| Beta-Estradiol | Sigma | E8875 |
| TMR-Poly-P Peptide | MIT core facility | N/A |
| TMR-Poly-E Peptide | MIT core facility | N/A |
| Critical Commercial Assays | | |
| Dual-glo Luciferase Assay System | Promega | E2920 |
| AllPrep DNA/RNA Mini Kit | QIAGEN | 80204 |
| NEBuilder HiFi DNA Assembly Master Mix | NEB | E2621S |
| Power SYBR Green mix | Life Technologies | 4367659 |
| Deposited Data | | |
| Oct4-degron + DMSO ChIP-seq | This Paper | GEO: GSM3401065 |
| Oct4-degron + dTag ChIP-seq | This Paper | GEO: GSM3401066 |
| Oct4-degron + DMSO ChIP-seq | This Paper | GEO: GSM3401067 |
| Oct4-degron + dTag ChIP-seq | This Paper | GEO: GSM3401068 |
| Oct4-degron + DMSO ChIP-Seq Input | This Paper | GEO: GSM3401069 |
| Oct4-degron + dTag ChIP-Seq Input | This Paper | GEO: GSM3401070 |
| Oct4-degron + DMSO RNA-seq | This Paper | GEO: GSM3401252 GEO: GSM3401253 |
| Oct4-degron + dTag RNA-seq | This Paper | GEO: GSM3401254 GEO: GSM3401255 |
| ES Cell RNA-seq | This Paper | GEO: GSM3401256 GEO: GSM3401257 |
| Differentiating ES Cell RNA-seq | This Paper | GEO: GSM3401258 GEO: GSM3401259 |
| Oct4 ChIP-Seq | Whyte et al., 2013 | GEO: GSM1082340 |
| Med1 ChIP-seq | Whyte et al., 2013 | GEO: GSM560348 |
| Experimental Models: Cell Lines | | |
| V6.5 murine embryonic stem cells | Jaenisch laboratory | N/A |
| HEK293T cells | ATCC | CRL-3216 |
| U2OS-268 cells | Spector laboratory | N/A |
| Oligonucleotides | | |
| mir290_Neg_F GGACTCCATCCCTAGTATTTGC | Operon | N/A |
| mir290_Neg_R GCTAATCACAAATTTGCTCTGC | Operon | N/A |
| mir290_OCT4_F CCACCTAAACAAAGAACAGCAG | Operon | N/A |
| mir290_OCT4_R TGTACCCTGCCACTCAGTTTAC | Operon | N/A |

(Continued on next page)

Continued

| REAGENT or RESOURCE | SOURCE | IDENTIFIER |
|--------------------------------------|---|---|
| mir290_MED1_F AAGCAGGGTGGTAGAGTAAGGA | Operon | N/A |
| mir290_MED1_R ATTCCCGATGTGGAGTAGAAGT | Operon | N/A |
| Recombinant DNA | | |
| pETEC-OCT4-GFP | This Paper | N/A |
| pETEC-MED1-IDR-GFP | Sabari et al., 2018. | N/A |
| pETEC-MED1-IDR-mCherry | Sabari et al., 2018. | N/A |
| pETEC-MED1-IDRXL-mCherry | This Paper | N/A |
| pETEC-OCT4-aromaticmutant-GFP | This Paper | N/A |
| pETEC-OCT4-acidicmutant-GFP | This Paper | N/A |
| pETEC-p53-GFP | This Paper | N/A |
| pETEC-yeast-MED15-mCherry | This Paper | N/A |
| pETEC-GCN4-GFP | This Paper | N/A |
| pETEC-GCN4-aromaticmutant-GFP | This Paper | N/A |
| pETEC-cMYC-GFP | This Paper | N/A |
| pETEC-NANOG-GFP | This Paper | N/A |
| pETEC-SOX2-GFP | This Paper | N/A |
| pETEC-RARa-GFP | This Paper | N/A |
| pETEC-GATA2-GFP | This Paper | N/A |
| pETEC-ER-GFP | This Paper | N/A |
| Lac-CFP-Empty | This Paper | N/A |
| Lac-GFP-Gcn4-AD | This Paper | N/A |
| Lac-GFP-Gcn4-AD-aromaticmutant | This Paper | N/A |
| pGL3BEC | Modified from Promega | N/A |
| pRLSV40 | Promega | N/A |
| pGal-DBD | This Paper | N/A |
| pGal-DBD-Oct4-C-AD | This Paper | N/A |
| pGal-DBD-Oct4-C-AD-acidicmutant | This Paper | N/A |
| pGal-DBD-GCN4-AD | This Paper | N/A |
| pGal-DBD-GCN4-AD-aromaticmutant | This Paper | N/A |
| pUC19-OCT4-FKBP-BFP | This Paper | N/A |
| pUC19-OCT4-FKBP-mcherry | This Paper | N/A |
| pX330-GFP-OCT4 | This Paper | N/A |
| Software and Algorithms | | |
| Fiji image processing package | Schindelin et al., 2012 | https://fiji.sc/ |
| MetaMorph acquisition software | Molecular Devices | https://www.moleculardevices.com/products/cellular-imaging-systems/acquisition-and-analysis-software/metamorph-microscopy |
| localCIDER package | Holehouse et al., 2017 | N/A |
| PONDR | http://www.pondr.com/ | N/A |
| Other | | |
| Esrrb RNA FISH probe | Stellaris | N/A |
| Nanog RNA FISH probe | Stellaris | N/A |
| miR290 RNA FISH probe | Stellaris | N/A |
| Trim28 RNA FISH probe | Stellaris | N/A |
| Nanog DNA FISH probe | Agilent | N/A |
| Mir290 DNA FISH probe | Agilent | N/A |

CONTACT FOR REAGENT AND RESOURCE SHARING

Further information and requests for resources and reagents should be directed to and will be fulfilled by the Lead Contact, Richard A. Young (young@wi.mit.edu).

EXPERIMENTAL MODEL AND SUBJECT DETAILS

Cells

V6.5 murine embryonic stem were a gift from R. Jaenisch of the Whitehead Institute. V6.5 are male cells derived from a C57BL/6(F) x 129/sv(M) cross. HEK293T cells were purchased from ATCC (ATCC CRL-3216). Cells were negative for mycoplasma.

Cell culture conditions

V6.5 murine embryonic stem (mES) cells were grown in 2i + LIF conditions. mES cells were always grown on 0.2% gelatinized (Sigma, G1890) tissue culture plates. The media used for 2i + LIF media conditions is as follows: 967.5 mL DMEM/F12 (GIBCO 11320), 5 mL N2 supplement (GIBCO 17502048), 10 mL B27 supplement (GIBCO 17504044), 0.5mM L-glutamine (GIBCO 25030), 0.5X non-essential amino acids (GIBCO 11140), 100 U/mL Penicillin-Streptomycin (GIBCO 15140), 0.1 mM β -mercaptoethanol (Sigma), 1 μ M PD0325901 (Stemgent 04-0006), 3 μ M CHIR99021 (Stemgent 04-0004), and 1000 U/mL recombinant LIF (ESGRO ESG1107). For differentiation mESCs were cultured in serum media as follows: DMEM (Invitrogen, 11965-092) supplemented with 15% fetal bovine serum (Hyclone, characterized SH3007103), 100 mM nonessential amino acids (Invitrogen, 11140-050), 2 mM L-glutamine (Invitrogen, 25030-081), 100 U/mL penicillin, 100 mg/mL streptomycin (Invitrogen, 15140-122), and 0.1mM β -mercaptoethanol (Sigma Aldrich). HEK293T cells were purchased from ATCC (ATCC CRL-3216) and cultured in DMEM, high glucose, pyruvate (GIBCO 11995-073) with 10% fetal bovine serum (Hyclone, characterized SH3007103), 100 U/mL Penicillin-Streptomycin (GIBCO 15140), 2 mM L-glutamine (Invitrogen, 25030-081). Cells were negative for mycoplasma.

METHOD DETAILS

Immunofluorescence with RNA FISH

Coverslips were coated at 37°C with 5 μ g/mL poly-L-ornithine (Sigma-Aldrich, P4957) for 30 minutes and 5 μ g/mL of Laminin (Corning, 354232) for 2 hours. Cells were plated on the pre-coated coverslips and grown for 24 hours followed by fixation using 4% paraformaldehyde, PFA, (VWR, BT140770) in PBS for 10 minutes. After washing cells three times in PBS, the coverslips were put into a humidifying chamber or stored at 4°C in PBS. Permeabilization of cells were performed using 0.5% Triton X-100 (Sigma Aldrich, X100) in PBS for 10 minutes followed by three PBS washes. Cells were blocked with 4% IgG-free Bovine Serum Albumin, BSA, (VWR, 102643-516) for 30 minutes and the indicated primary antibody (see table S2) was added at a concentration of 1:500 in PBS for 4-16 hours. Cells were washed with PBS three times followed by incubation with secondary antibody at a concentration of 1:5000 in PBS for 1 hour. After washing twice with PBS, cells were fixed using 4% paraformaldehyde, PFA, (VWR, BT140770) in PBS for 10 minutes. After two washes of PBS, Wash buffer A (20% Stellaris RNA FISH Wash Buffer A (Biosearch Technologies, Inc., SMF-WA1-60), 10% Deionized Formamide (EMD Millipore, S4117) in RNase-free water (Life Technologies, AM9932) was added to cells and incubated for 5 minutes. 12.5 μ M RNA probe (Table S4, Stellaris) in Hybridization buffer (90% Stellaris RNA FISH Hybridization Buffer (Biosearch Technologies, SMF-HB1-10) and 10% Deionized Formamide) was added to cells and incubated overnight at 37°C. After washing with Wash buffer A for 30 minutes at 37°C, the nuclei were stained with 20 μ M/mL Hoechst 33258 (Life Technologies, H3569) for 5 minutes, followed by a 5 minute wash in Wash buffer B (Biosearch Technologies, SMF-WB1-20). Cells were washed once in water followed by mounting the coverslip onto glass slides with Vectashield (VWR, 101098-042) and finally sealing the coverslip with nail polish (Electron Microscopy Science Nm, 72180). Images were acquired at an RPI Spinning Disk confocal microscope with a 100x objective using MetaMorph acquisition software and a Hamamatsu ORCA-ER CCD camera (W.M. Keck Microscopy Facility, MIT). Images were post-processed using Fiji Is Just ImageJ (FIJI).

Immunofluorescence with DNA FISH

Immunofluorescence was performed as previously described above. After incubating the cells with the secondary antibodies, cells were washed three times in PBS for 5min at RT, fixed with 4% PFA in PBS for 10min and washed three times in PBS. Cells were incubated in 70% ethanol, 85% ethanol and then 100% ethanol for 1 minute at RT. Probe hybridization mixture was made mixing 7 μ L of FISH Hybridization Buffer (Agilent G9400A), 1 μ L of FISH probe (see below for region) and 2 μ L of water. 5 μ L of mixture was added on a slide and coverslip was placed on top (cell-side toward the hybridization mixture). Coverslips were sealed using rubber cement. Once rubber cement solidified, genomic DNA and probes were denatured at 78°C for 5 minutes and slides were incubated at 16°C in the dark O/N. The coverslip was removed from the slide and incubated in pre-warmed Wash buffer 1 (Agilent, G9401A) at 73°C for 2 minutes and in Wash Buffer 2 (Agilent, G9402A) for 1 minute at RT. Slides were air dried and nuclei were stained with Hoechst in PBS for 5 minutes at RT. Coverslips were washed three times in PBS, mounted on slides using Vectashield and

sealed with nail polish. Images were acquired on an RPI Spinning Disk confocal microscope with a 100x objective using MetaMorph acquisition software and a Hamamatsu ORCA-ER CCD camera (W.M. Keck Microscopy Facility, MIT). Images were post-processed using FIJI.

DNA FISH probes were custom designed and generated by Agilent to target Nanog and MiR290 super enhancers.

Nanog

Design Input Region – mm9

chr6 122605249 – 122705248

Design Region – mm9

chr6: 122605985-122705394

Mir290

Design Region – mm10

chr7: 3141151 – 3241381

Tissue culture

V6.5 murine embryonic stem cells (mESCs) were a gift from the Jaenisch lab. Cells were grown on 0.2% gelatinized (Sigma, G1890) tissue culture plates in 2i media (DMEM-F12 (Life Technologies, 11320082), 0.5X B27 supplement (Life Technologies, 17504044), 0.5X N2 supplement (Life Technologies, 17502048), an extra 0.5mM L-glutamine (GIBCO, 25030-081), 0.1mM b-mercaptoethanol (Sigma, M7522), 1% Penicillin Streptomycin (Life Technologies, 15140163), 0.5X nonessential amino acids (GIBCO, 11140-050), 1000 U/ml LIF (Chemico, ESG1107), 1 μ M PD0325901 (Stemgent, 04-0006-10), 3 μ M CHIR99021 (Stemgent, 04-0004-10)). Cells were grown at 37°C with 5% CO₂ in a humidified incubator. For confocal imaging, cells were grown on glass coverslips (Carolina Biological Supply, 633029), coated with 5 μ g/mL of poly-L-ornithine (Sigma Aldrich, P4957) for 30 minutes at 37°C and with 5 μ g/ml of Laminin (Corning, 354232) for 2hrs-16hrs at 37°C. For passaging, cells were washed in PBS (Life Technologies, AM9625), 1000 U/mL LIF. TrypLE Express Enzyme (Life Technologies, 12604021) was used to detach cells from plates. TrypLE was quenched with FBS/LIF-media ((DMEM K/O (GIBCO, 10829-018), 1X nonessential amino acids, 1% Penicillin Streptomycin, 2mM L-Glutamine, 0.1mM b-mercaptoethanol and 15% Fetal Bovine Serum, FBS, (Sigma Aldrich, F4135)). Cells were spun at 1000rpm for 3 minutes at RT, resuspended in 2i media and 5x10⁶ cells were plated in a 15 cm dish. For differentiation of mESCs, 6000 cells were plated per well of a 6 well tissue culture dish, or 1000 cells were plated per well of a 24 well plate with a laminin coated glass coverslip. After 24 hours, 2i media was replaced with FBS media (above) without LIF. Media was changed daily for 5 days, cells were then harvested.

Western blot

Cells were lysed in Cell Lytic M (Sigma-Aldrich C2978) with protease inhibitors (Roche, 11697498001). Lysate was run on a 3%–8% Tris-acetate gel or 10% Bis-Tris gel or 3%–8% Bis-Tris gels at 80 V for ~2 hr, followed by 120 V until dye front reached the end of the gel. Protein was then wet transferred to a 0.45 μ m PVDF membrane (Millipore, IPVH00010) in ice-cold transfer buffer (25 mM Tris, 192 mM glycine, 10% methanol) at 300 mA for 2 hours at 4°C. After transfer the membrane was blocked with 5% non-fat milk in TBS for 1 hour at room temperature, shaking.

Membrane was then incubated with 1:1,000 of the indicated antibody (Table S2) diluted in 5% non-fat milk in TBST and incubated overnight at 4°C, with shaking. In the morning, the membrane was washed three times with TBST for 5 minutes at room temperature shaking for each wash. Membrane was incubated with 1:5,000 secondary antibodies for 1 hr at RT and washed three times in TBST for 5 minutes. Membranes were developed with ECL substrate (Thermo Scientific, 34080) and imaged using a CCD camera or exposed using film or with high sensitivity ECL.

Chromatin immunoprecipitation (ChIP) qPCR and sequencing

mES were grown to 80% confluence in 2i media. 1% formaldehyde in PBS was used for crosslinking of cells for 15 minutes, followed by quenching with Glycine at a final concentration of 125mM on ice. Cells were washed with cold PBS and harvested by scraping cells in cold PBS. Collected cells were pelleted at 1000 g for 3 minutes at 4°C, flash frozen in liquid nitrogen and stored at –80°C. All buffers contained freshly prepared cOmplete protease inhibitors (Roche, 11873580001). Frozen crosslinked cells were thawed on ice and then resuspended in lysis buffer I (50 mM HEPES-KOH, pH 7.5, 140 mM NaCl, 1 mM EDTA, 10% glycerol, 0.5% NP-40, 0.25% Triton X-100, protease inhibitors) and rotated for 10 minutes at 4°C, then spun at 1350 rcf., for 5 minutes at 4°C. The pellet was resuspended in lysis buffer II (10 mM Tris-HCl, pH 8.0, 200 mM NaCl, 1 mM EDTA, 0.5 mM EGTA, protease inhibitors) and rotated for 10 minutes at 4°C and spun at 1350 rcf. for 5 minutes at 4°C. The pellet was resuspended in sonication buffer (20 mM Tris-HCl pH 8.0, 150 mM NaCl, 2 mM EDTA pH 8.0, 0.1% SDS, and 1% Triton X-100, protease inhibitors) and then sonicated on a Misonix 3000 sonicator for 10 cycles at 30 s each on ice (18–21 W) with 60 s on ice between cycles. Sonicated lysates were cleared once by centrifugation at 16,000 rcf. for 10 minutes at 4°C. Input material was reserved and the remainder was incubated overnight at 4°C with magnetic beads bound with antibody (Table S2) to enrich for DNA fragments bound by the indicated factor. Beads were washed twice with each of the following buffers: wash buffer A (50 mM HEPES-KOH pH 7.5, 140 mM NaCl, 1 mM EDTA pH 8.0,

0.1% Na-Deoxycholate, 1% Triton X-100, 0.1% SDS), wash buffer B (50 mM HEPES-KOH pH 7.9, 500 mM NaCl, 1 mM EDTA pH 8.0, 0.1% Na-Deoxycholate, 1% Triton X-100, 0.1% SDS), wash buffer C (20 mM Tris-HCl pH 8.0, 250 mM LiCl, 1 mM EDTA pH 8.0, 0.5% Na-Deoxycholate, 0.5% IGEPAL C-630, 0.1% SDS), wash buffer D (TE with 0.2% Triton X-100), and TE buffer. DNA was eluted off the beads by incubation at 65°C for 1 hour with intermittent vortexing in elution buffer (50 mM Tris-HCl pH 8.0, 10 mM EDTA, 1% SDS). Cross-links were reversed overnight at 65°C. To purify eluted DNA, 200 μ L TE was added and then RNA was degraded by the addition of 2.5 μ L of 33 mg/mL RNase A (Sigma, R4642) and incubation at 37°C for 2 hours. Protein was degraded by the addition of 10 μ L of 20 mg/mL proteinase K (Invitrogen, 25530049) and incubation at 55°C for 2 hours. A phenol:chloroform:isoamyl alcohol extraction was performed followed by an ethanol precipitation. The DNA was then resuspended in 50 μ L TE and used for either qPCR or sequencing. For ChIP-qPCR experiments, qPCR was performed using Power SYBR Green mix (Life Technologies #4367659) on either a QuantStudio 5 or a QuantStudio 6 System (Life Technologies).

RNA-Seq

RNA-Seq was performed in the indicated cell line with the indicated treatment, and used to determine expressed genes. RNA was isolated by AllPrep Kit (QIAGEN 80204) and polyA selected libraries were prepared using the KAPA mRNA HyperPrep Kit (Kapa Biosystems KK8505) according to manufacturer's protocol, and single-end sequenced on a Hi-seq 2500 instrument.

Protein purification

cDNA encoding the genes of interest or their IDRs were cloned into a modified version of a T7 pET expression vector. The base vector was engineered to include a 5' 6xHIS followed by either mEGFP or mCherry and a 14 amino acid linker sequence "GAPGSAGSAAGGSG." NEBuilder® HiFi DNA Assembly Master Mix (NEB E2621S) was used to insert these sequences (generated by PCR) in-frame with the linker amino acids. Vectors expressing mEGFP or mCherry alone contain the linker sequence followed by a STOP codon. Mutant sequences were synthesized as geneblocks (IDT) and inserted into the same base vector as described above. All expression constructs were sequenced to ensure sequence identity. For protein expression, plasmids were transformed into LOBSTR cells (gift of Chessman Lab) and grown as follows. A fresh bacterial colony was inoculated into LB media containing kanamycin and chloramphenicol and grown overnight at 37°C. Cells containing the MED1-IDR constructs were diluted 1:30 in 500ml room temperature LB with freshly added kanamycin and chloramphenicol and grown 1.5 hours at 16°C. IPTG was added to 1mM and growth continued for 18 hours. Cells were collected and stored frozen at -80°C. Cells containing all other constructs were treated in a similar manner except they were grown for 5 hours at 37°C after IPTG induction.

Pellets of 500ml of cMyc and Nanog cells were resuspended in 15ml of denaturing buffer (50mM Tris 7.5, 300mM NaCl, 10mM imidazole, 8M Urea) containing cOmplete protease inhibitors (Roche,11873580001) and sonicated (ten cycles of 15 s on, 60 s off). The lysates were cleared by centrifugation at 12,000 g for 30 minutes and added to 1ml of Ni-NTA agarose (Invitrogen, R901-15) that had been pre-equilibrated with 10 volumes of the same buffer. Tubes containing this agarose lysate slurry were rotated for 1.5 hours. The slurry was poured into a column, washed with 15 volumes of the lysis buffer and eluted 4 X with denaturing buffer containing 250mM imidazole. Each fraction was run on a 12% gel and proteins of the correct size were dialyzed first against buffer (50mM Tris pH 7.5, 125mM NaCl, 1mM DTT and 4M Urea), followed by the same buffer containing 2M Urea and lastly 2 changes of buffer with 10% Glycerol, no Urea. Any precipitate after dialysis was removed by centrifugation at 3,000rpm for 10 minutes. All other proteins were purified in a similar manner. 500ml cell pellets were resuspended in 15ml of Buffer A (50mM Tris pH7.5, 500 mM NaCl) containing 10mM imidazole and cOmplete protease inhibitors, sonicated, lysates cleared by centrifugation at 12,000 g for 30 minutes at 4°C, added to 1ml of pre-equilibrated Ni-NTA agarose, and rotated at 4°C for 1.5 hours. The slurry was poured into a column, washed with 15 volumes of Buffer A containing 10mM imidazole and protein was eluted 2 X with Buffer A containing 50mM imidazole, 2 X with Buffer A containing 100mM imidazole, and 3 X with Buffer A containing 250mM imidazole. Alternatively, the resin slurry was centrifuged at 3,000rpm for 10 minutes, washed with 15 volumes of Buffer and proteins were eluted by incubation for 10 or more minutes rotating with each of the buffers above (50mM, 100mM and 250mM imidazole) followed by centrifugation and gel analysis. Fractions containing protein of the correct size were dialyzed against two changes of buffer containing 50mM Tris 7.5, 125mM NaCl, 10% glycerol and 1mM DTT at 4°C.

In vitro droplet assay

Recombinant GFP or mCherry fusion proteins were concentrated and desalted to an appropriate protein concentration and 125mM NaCl using Amicon Ultra centrifugal filters (30K MWCO, Millipore). Recombinant proteins were added to solutions at varying concentrations with indicated final salt and 10% PEG-8000 as crowding agent in Droplet Formation Buffer (50mM Tris-HCl pH 7.5, 10% glycerol, 1mM DTT). The protein solution was immediately loaded onto a homemade chamber comprising a glass slide with a coverslip attached by two parallel strips of double-sided tape. Slides were then imaged with an Andor confocal microscope with a 150x objective. Unless indicated, images presented are of droplets settled on the glass coverslip. For experiments with fluorescently labeled polypeptides, the indicated decapeptides were synthesized by the Koch Institute/MIT Biopolymers & Proteomics Core Facility with a TMR fluorescent tag. The protein of interest was added Buffer D with 125mM NaCl and 10% Peg-8000 with the indicated polypeptide and imaged as described above. For FRAP of *in vitro* droplets 5 pulses of laser at a 50us dwell time was applied to the droplet, and recovery was imaged on an Andor microscope every 1 s for the indicated time periods. For estrogen stimulation experiments, fresh B-Estradiol (E8875 Sigma) was reconstituted to 10mM in 100% EtOH then diluted in 125mM NaCl droplet formation buffer to

100uM. One microliter of this concentrated stock was used in a 10uL droplet formation reaction to achieve a final concentration of 10uM.

Genome editing and protein degradation

The CRISPR/Cas9 system was used to genetically engineer ESC lines. Target-specific oligonucleotides were cloned into a plasmid carrying a codon-optimized version of Cas9 with GFP (gift from R. Jaenisch). The sequences of the DNA targeted (the protospacer adjacent motif is underlined) are listed in the same table. For the generation of the endogenously tagged lines, 1 million Med1-mEGFP tagged mES cells were transfected with 2.5 mg Cas9 plasmid containing the guide sequence below (pX330-GFP-Oct4) and 1.25 mg non-linearized repair plasmid 1 (pUC19-Oct4-FKBP-BFP) and 1.25 mg non-linearized repair plasmid 2 (pUC19-Oct4-FKBP-mcherry) (Table S3). Cells were sorted after 48 hours for the presence of GFP. Cells were expanded for five days and then sorted again for double positive mCherry and BFP cells. Forty thousand mCherry+/BFP+ sorted cells were plated in a six-well plate in a serial dilution. The cells were grown for approximately one week in 2i medium and then individual colonies were picked using a stereoscope into a 96-well plate. Cells were expanded and genotyped by PCR, degradation was confirmed by western blot and IF. Clones with a homozygous knock-in tag were further expanded and used for experiments. A clonal homozygous knock-in line expressing FKBP tagged Oct4 was used for the degradation experiments. Cells were grown in 2i and then treated with dTAG-47 at a concentration of 100 nM for 24 hours, then harvested.

Oct4 Guide sequence

tgcatcactgaggcacc*NGG(PAM)

GAL4 transcription assay

Transcription factor constructs were assembled in a mammalian expression vector containing an SV40 promoter driving expression of a GAL4 DNA-binding domain. Wild-type and mutant activation domains of *Oct4* and *Gcn4* were fused to the C terminus of the DNA-binding domain by Gibson cloning (NEB 2621S), joined by the linker GAPGSAGSAAGGSG. These transcription factor constructs were transfected using Lipofectamine 3000 (ThermoFisher L3000015) into HEK293T cells (ATCC CRL-3216) or V6.5 mouse embryonic stem cells, that were grown in white flat-bottom 96-well assay plates (Costar 3917). The transcription factor constructs were co-transfected with a modified version of the PGL3-Basic (Promega) vector containing five GAL4 upstream activation sites upstream of the firefly luciferase gene. Also co-transfected was pRL-SV40 (Promega), a plasmid containing the Renilla luciferase gene driven by an SV40 promoter. 24 hours after transfection, luminescence generated by each luciferase protein was measured using the Dual-glo Luciferase Assay System (Promega E2920). The data as presented has been controlled for Renilla luciferase expression.

Lac binding assay

Constructs were assembled by NEB HIFI cloning in pSV2 mammalian expression vector containing an SV40 promoter driving expression of a CFP-LacI fusion protein. The activation domains and mutant activation domains of *Gcn4* were fused by the c-terminus to this recombinant protein, joined by the linker sequence GAPGSAGSAAGGSG. U2OS-268 cells containing a stably integrated array of ~51,000 Lac-repressor binding sites (a gift of the Spector laboratory) were transfected using lipofectamine 3000 (ThermoFisher L3000015). 24 hours after transfection, cells were plated on fibronectin-coated glass coverslips. After 24 hours on glass coverslips, cells were fixed for immunofluorescence with a MED1 antibody (Table S2) as described above and imaged, by spinning disk confocal microscopy.

Purification of CDK8-Mediator

The CDK8-Mediator samples were purified as described (Meyer et al., 2008) with modifications. Prior to affinity purification, the P0.5M/QFT fraction was concentrated, to 12 mg/mL, by ammonium sulfate precipitation (35%). The pellet was resuspended in pH 7.9 buffer containing 20 mM KCl, 20mM HEPES, 0.1mM EDTA, 2mM MgCl₂, 20% glycerol and then dialyzed against pH 7.9 buffer containing 0.15M KCl, 20mM HEPES, 0.1mM EDTA, 20% glycerol and 0.02% NP-40 prior to the affinity purification step. Affinity purification was carried out as described (Meyer et al., 2008), eluted material was loaded onto a 2.2mL centrifuge tube containing 2mL 0.15M KCl HEMG (20mM HEPES, 0.1mM EDTA, 2mM MgCl₂, 10% glycerol) and centrifuged at 50K RPM for 4h at 4°C. This served to remove excess free GST-SREBP and to concentrate the CDK8-Mediator in the final fraction. Prior to droplet assays, purified CDK8-Mediator was concentrated using Microcon-30kDa Centrifugal Filter Unit with Ultracel-30 membrane (Millipore MRCF0R030) to reach ~300nM of Mediator complex. Concentrated CDK8-Mediator was added to the droplet assay to a final concentration of ~200nM with or without 10 μM indicated GFP-tagged protein. Droplet reactions contained 10% PEG-8000 and 140mM salt.

QUANTIFICATION AND STATISTICAL ANALYSIS

Experimental design

All experiments were replicated. For the specific number of replicates done see either the figure legends or the specific section below. No aspect of the study was done blinded. Sample size was not predetermined and no outliers were excluded.

Average image and radial distribution analysis

For analysis of RNA FISH with immunofluorescence custom in-house MATLAB scripts were written to process and analyze 3D image data gathered in FISH (RNA/DNA) and IF channels. FISH foci were manually identified in individual z stacks through intensity thresholds, centered along a box of size $l = 2.9 \mu m$, and stitched together in 3-D across z stacks. The called FISH foci are cross-referenced against a manually curated list of FISH foci to remove false positives, which arise due to extra-nuclear signal or blips. For every RNA FISH focus identified, signal from the corresponding location in the IF channel is gathered in the $l \times l$ square centered at the RNA FISH focus at every corresponding z-slice. The IF signal centered at FISH foci for each FISH and IF pair are then combined and an average intensity projection is calculated, providing averaged data for IF signal intensity within a $l \times l$ square centered at FISH foci. The same process was carried out for the FISH signal intensity centered on its own coordinates, providing averaged data for FISH signal intensity within a $l \times l$ square centered at FISH foci. As a control, this same process was carried out for IF signal centered at randomly selected nuclear positions. Randomly selected nuclear positions were identified for each image set by first identifying nuclear volume and then selecting positions within that volume. Nuclear volumes were determined from DAPI staining through the z stack image, which was then processed through a custom CellProfiler pipeline (included as auxiliary file). Briefly, this pipeline rescales the image intensity, condenses the image to 20% of original size for speed of processing, enhances detected speckles, filters median signal, thresholds bodies, removes holes, filters the median signal, dilates the image back to original size, watersheds nuclei, and converts the resulting objects into a black and white image. This black and white image is used as input for a custom R script that uses readTIFF and im (from spatstat) to select 40 random nuclear voxels per image set. These average intensity projections were then used to generate 2D contour maps of the signal intensity or radial distribution plots. Contour plots are generated using in-built functions in MATLAB. The intensity radial function ($I(r)$) is computed from the average data. For the contour plots, the intensity-color ranges presented were customized across a linear range of colors ($n! = 15$). For the FISH channel, black to magenta was used. For the IF channel, we used chroma.js (an online color generator) to generate colors across 15 bins, with the key transition colors chosen as black, blueviolet, mediumblue, lime. This was done to ensure that the reader's eye could more readily detect the contrast in signal. The generated colormap was employed to 15 evenly spaced intensity bins for all IF plots. The averaged IF centered at FISH or at randomly selected nuclear locations are plotted using the same color scale, set to include the minimum and maximum signal from each plot. For DNA FISH analysis FISH foci were manually identified in individual z stacks through intensity thresholds in FIJI and marked as a reference area. The reference areas were then transferred to the MED1 IF channel of the image and the average IF signal within the FISH focus was determined. The average signal across 5 images comprising greater than 10 cells per image was averaged to calculate the mean MED1 IF intensity associated with the DNA FISH focus.

Chromatin immunoprecipitation PCR and sequencing (ChIP) analysis

Values displayed in the figures were normalized to the input. The average WT normalized values and standard deviation are displayed. The primers used are listed below. ChIP values at the region of interest (ROI) were normalized to input values (fold input) and for the *mir290* enhancer an additional negative region (negative norm). Values are displayed as normalized to the ES state in differentiation experiments and to DMSO control in OCT4 degradation experiments (control normalization). qPCR reactions were performed in technical triplicate.

$$\text{Fold input} = 2^{(Ct_{input} - Ct_{ChIP})}$$

$$\text{Negative norm} = \frac{\text{Fold input}_{ROI}}{\text{Fold input}_{neg}}$$

$$\text{Control norm(Differentiation)} = \frac{\text{Neg norm}_{Differentiated}}{\text{Neg norm}_{ES}}$$

ChIP qPCR Primers

Mir290

mir290_Neg_F GGA^{CT}CCATCCCTAGTATTTGC
 mir290_Neg_R GCTAATCACA^{AATTTGCTCTGC}
 mir290_OCT4_F CCACCTAAACA^{AAGAACAGCAG}
 mir290_OCT4_R TGTACCCTGCCACTCAGTTTAC
 mir290_MED1_F AAGCAGGGTGGTAGAGTAAGGA
 mir290_MED1_R ATTCCCGATGTGGAGTAGAAGT

ChIP-Seq data were aligned to the mm9 version of the mouse reference genome using bowtie with parameters $-k\ 1 -m\ 1 -best$ and $-l$ set to read length. Wiggle files for display of read coverage in bins were created using MACS with parameters $-w -S -space = 50 -nomodel -shiftsize = 200$, and read counts per bin were normalized to the millions of mapped reads used to make the wiggle file. Reads-per-million-normalized wiggle files were displayed in the UCSC genome browser. ChIP-Seq tracks shown in Figure 1 are derived from GEO: GSM1082340 (OCT4) and GEO: GSM560348 (MED1) from Whyte et al. (2013). Super-enhancers and typical enhancers and their associated genes in cells grown in 2i conditions were downloaded from Sabari et al., 2018. Distributions of occupancy fold-changes were calculated using bamToGFF (<https://github.com/BradnerLab/pipeline>) to quantify coverage in super-enhancers and typical enhancers from cells grown in 2i conditions. Reads overlapping each typical and super-enhancer were determined using bamToGFF with parameters $-e\ 200 -f\ 1 -t\ TRUE$ and were subsequently normalized to the millions of mapped reads (RPM). RPM-normalized input read counts from each condition were then subtracted from RPM-normalized ChIP-Seq read counts from the corresponding condition. Values from regions wherein this subtraction resulted in a negative number were set to 0. Log₂ fold-changes were calculated between DMSO-treated (normal OCT4 amount) and dTAG-treated (depleted OCT4); one pseudocount was added to each condition.

Super-enhancer identification

Super-enhancers were identified as described in Whyte et al. (2013). Peaks of enrichment in MED1 were identified using MACS with $-p\ 1e-9 -keep-dup = 1$ and input control. MED1 aligned reads from the untreated condition and corresponding peaks of MED1 were used as input for ROSE (https://bitbucket.org/young_computation/) with parameters $-s\ 12500 -t\ 2000 -g\ mm9$ and input control. A custom gene list was created by adding D7Erd143e, and removing Mir290, Mir291a, Mir291b, Mir292, Mir293, Mir294, and Mir295 to prevent these nearby microRNAs that are part of the same transcript from being multiply counted. Stitched enhancers (super-enhancers and typical enhancers) were assigned to the single expressed RefSeq transcript whose promoter was nearest the center of the stitched enhancer. Expressed transcripts were defined as above.

RNA-Seq analysis

For analysis, raw reads were aligned to the mm9 revision of the mouse reference genome using hisat2 with default parameters. Gene name-level read count quantification was performed with htseq-count with parameters $-l\ gene_id -stranded = reverse -f\ bam -m\ intersection-strict$ and a GTF containing transcript positions from Refseq, downloaded 6/6/18. Normalized counts, normalized fold-changes, and differential expression p values were determined using DEseq2 using the standard workflow and both replicates of each condition.

Enrichment and charge analysis of OCT4

Amino acid composition plots were generated using R by plotting the amino acid identity of each residue along the amino acid sequence of the protein. Net charge per residue for OCT4 was determined by computing the average amino acid charge along the OCT4 amino acid sequence in a 5 amino acid sliding window using the localCIDER package (Holehouse et al., 2017).

Disorder enrichment analysis

A list of human transcription factors protein sequences is used for all analysis on TFs, as defined in (Saint-andré et al., 2016). The reference human proteome (Uniprot UP000005640) is used to distill the list (down to ~1200 proteins), mostly removing non-canonical isoforms. Transcriptional coactivators and Pol II associated proteins were identified in humans using the GO enrichments IDS GO:0003713 and GO:0045944. The reference human proteome defined above was used to generate list of all human proteins, and peroxisome and Golgi proteins were identified from Uniprot reviewed lists. For each protein, D2P2 was used to assay disorder propensity for each amino acid. An amino acid in a protein is considered disordered if at least 75% of the algorithms employed by D2P2 (Oates et al., 2013) predict the residue to be disordered. Additionally, for transcription factors, all annotated PFAM domains were identified (5741 in total, 180 unique domains). Cross-referencing PFAM annotation for known DNA-binding activity, a subset of 45 unique high-confidence DNA-binding domains were identified, accounting for ~85% of all identified domains. The vast majority of TFs (> 95%) had at least one identified DNA-binding domain. Disorder scores were computed for all DNA-binding regions in every TF, as well as the remaining part of the sequence, which includes most identified trans-activation domains.

Imaging analysis of *in vitro* droplets

To analyze *in-vitro* phase separation imaging experiments, custom MATLAB scripts were written to identify droplets and characterize their size and shape. For any particular experimental condition, intensity thresholds based on the peak of the histogram and size thresholds (2 pixel radius) were employed to segment the image. Droplet identification was performed on the “scaffold” channel (MED1 in case of MED1 + TFs, GCN4 for GCN4+MED15), and areas and aspect ratios were determined. To calculate enrichment for the *in vitro* droplet assay, droplets were defined as a region of interest in FIJI by the scaffold channel, and the maximum signal of the client within that droplet was determined. Scaffolds chosen were MED1, Mediator complex, or GCN4. This was divided by the background client signal in the image to generate a Cin/out. Enrichment scores were calculated by dividing the Cin/out of the experimental condition by the Cin/out of a control fluorescent protein (either GFP or mCherry).

DATA AND SOFTWARE AVAILABILITY

Datasets

| Figure | Dataset type | IP target | Sample | GEO |
|---------------------------|----------------|-----------|-------------------------|---------------------------------|
| Figure 2B | ChIP-Seq | OCT4 | Oct4-degron + DMSO | GEO: GSM3401065 |
| Figure 2B | ChIP-Seq | OCT4 | Oct4-degron + dTag | GEO: GSM3401066 |
| Figure 2B | ChIP-Seq | MED1 | Oct4-degron + DMSO | GEO: GSM3401067 |
| Figure 2B | ChIP-Seq | MED1 | Oct4-degron + dTag | GEO: GSM3401068 |
| Figure 2B | ChIP-Seq Input | N/A | Oct4-degron + DMSO | GEO: GSM3401069 |
| Figure 2B | ChIP-Seq Input | N/A | Oct4-degron + dTag | GEO: GSM3401070 |
| Figure 2B | RNA-Seq | N/A | Oct4-degron + DMSO | GEO: GSM3401252 GEO: GSM3401253 |
| Figure 2B | RNA-Seq | N/A | Oct4-degron + dTag | GEO: GSM3401254 GEO: GSM3401255 |
| Figure 2H | RNA-Seq | N/A | ES Cell | GEO: GSM3401256 GEO: GSM3401257 |
| Figure 2H | RNA-Seq | N/A | Differentiating ES Cell | GEO: GSM3401258 GEO: GSM3401259 |

The overall accession number for the sequencing data reported in this paper is: GEO: GSE120476.

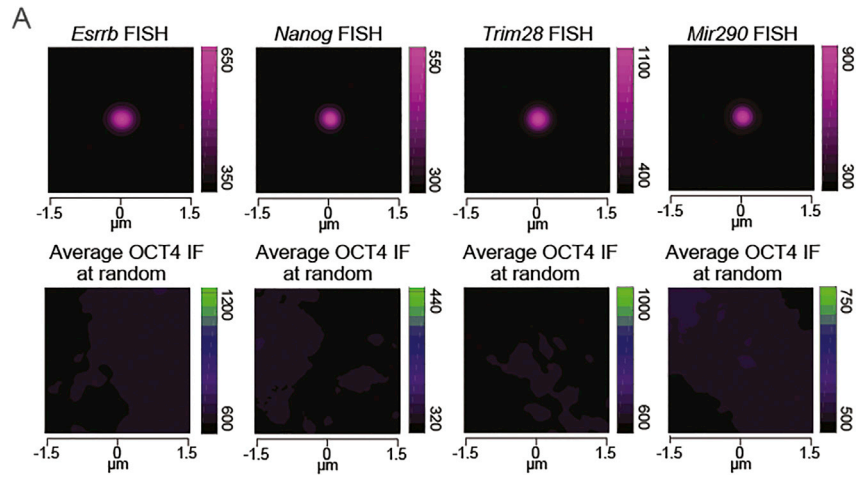


Figure S1. Random Focus Analysis, Related to Figure 1

Average fluorescence centered at the indicated RNA FISH focus (top panels) versus a randomly distributed IF foci ± 1.5 microns in X and Y (bottom panels). Color scale bars present arbitrary units of fluorescence intensity.

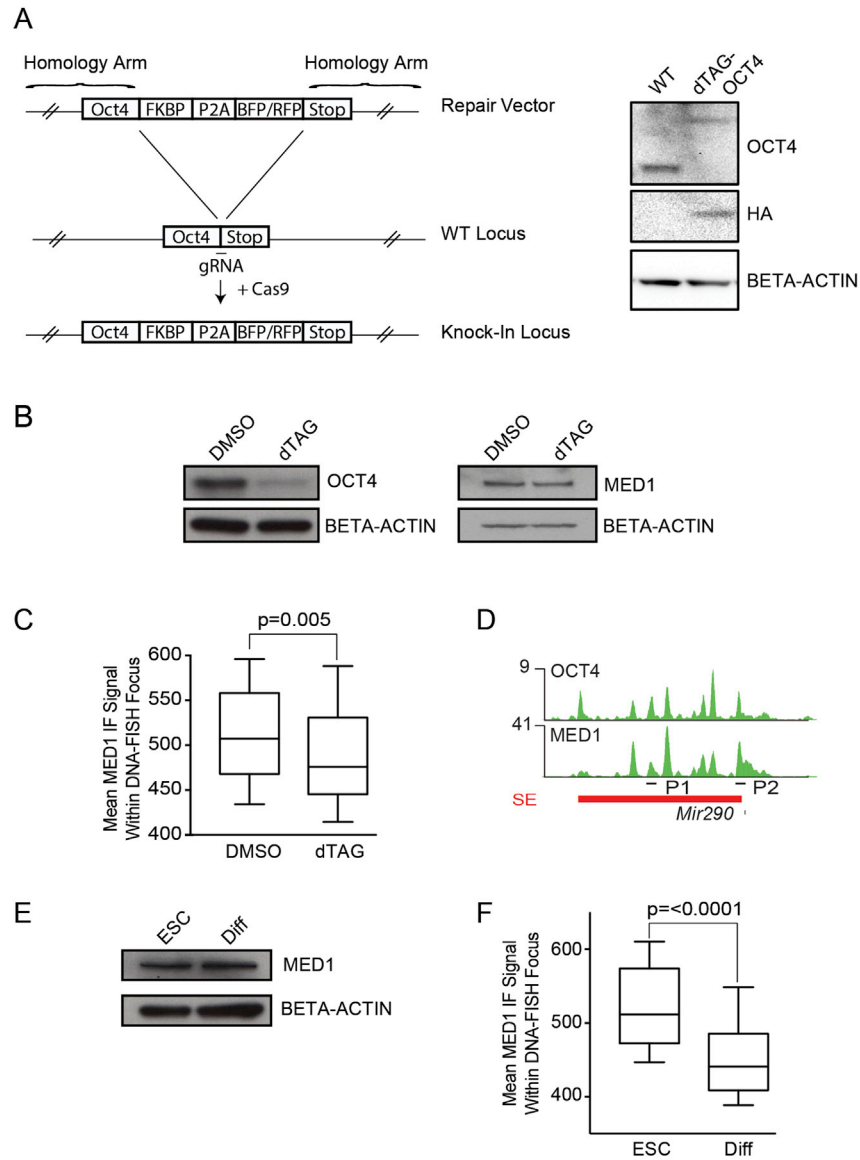


Figure S2. OCT4 Degradation and ES Cell Differentiation, Related to Figure 2

A. Schematic of the Oct4-FKBP cell-engineering strategy. V6.5 mouse ES cells were transfected with a repair vector and Cas9 expressing plasmid to generate knock-in loci with either BFP or RFP for selection (Left). WT or untreated OCT4-dTAG ES cells blotted for OCT4 showing expected shift in size, HA (on FKBP), and ACTIN (Right).

B. Western blot against OCT4 (left panels), MED1 (right panels), and BETA-ACTIN in the OCT4 degron line (dTAG), either treated with dTag47 or vehicle (DMSO).

C. Mean intensity of the MED1 IF signal within the Nanog DNA FISH focus in DMSO treated, versus dTAG treated OCT4-degron cells. n = 5 images, error bars are distribution between the 10th and 90th percentile.

D. Schematic showing the position of primers used for OCT4 (P1) and MED1 (P2) ChIP-qPCR in differentiated and ES cells at the Mir290 locus.

E. Western blot against MED1 and BETA-ACTIN in ES cells or cells differentiated by LIF withdrawal.

F. Mean intensity of MED1 IF signal within Mir290 DNA FISH focus in ES cells versus cells differentiated by LIF withdrawal. n = 5 images, error bars are distribution between the 10th and 90th percentile.

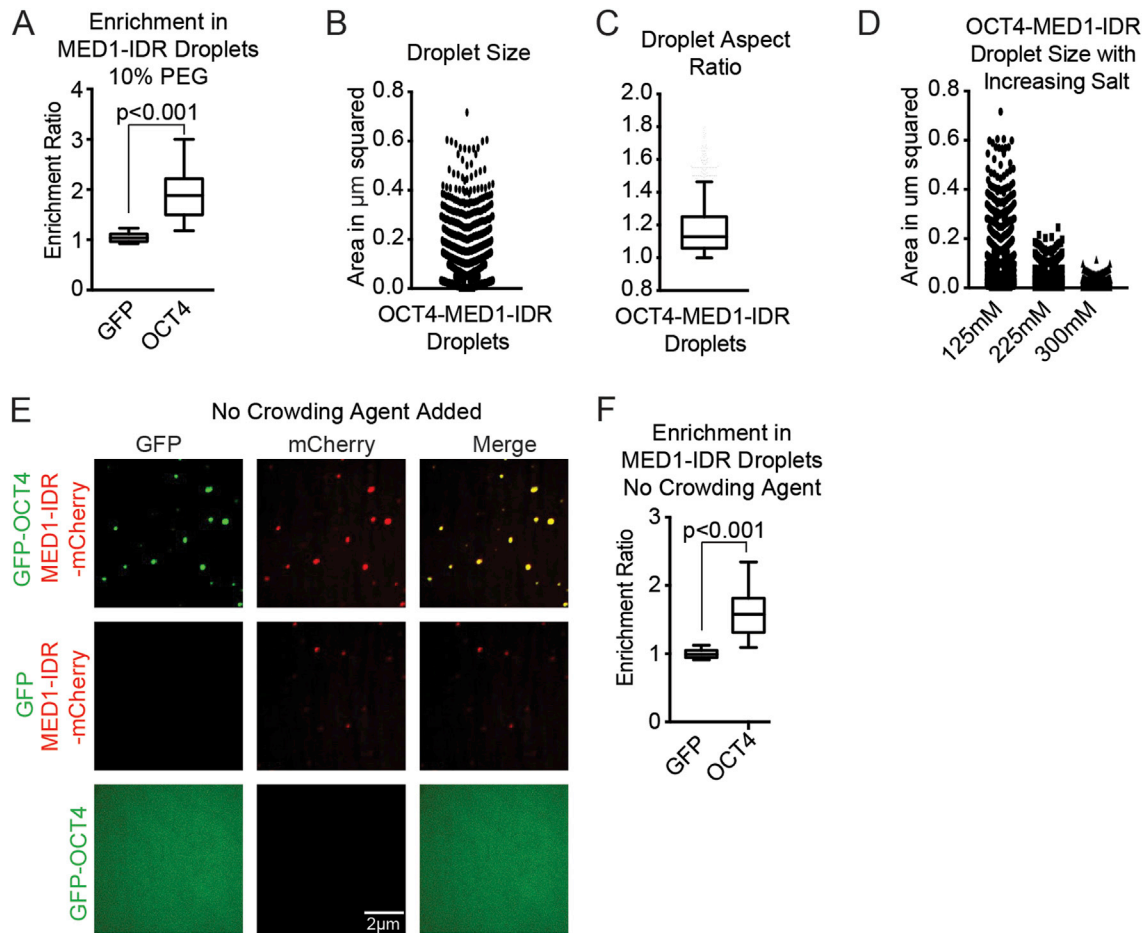


Figure S3. MED1 and OCT4 Droplet Formation, Related to Figure 3

A. Enrichment ratio of OCT4-GFP versus GFP in MED1-IDR-mCherry droplets formed in droplet formation buffer with 10% PEG-8000 at 125mM NaCl. $n > 20$, error bars represent the distribution between the 10th and 90th percentile.

B. Area in micrometers-squared of MED1-IDR-OCT4 droplets formed in 10% PEG-8000 at 125mM salt with 10 μM of each protein.

C. Aspect ratio of MED1-IDR-OCT4 droplets formed in 10% PEG-8000 at 125mM with 10 μM of each protein. $n > 20$, error bars represent the distribution between the 10th and 90th percentile.

D. Area in micrometers-squared of MED1-IDR-OCT4 droplets formed in 10% PEG-8000 at 125mM, 225 μM , or 300 μM salt, with 10 μM of each protein.

E. Fluorescence microscopy of droplet formation without crowding agents at 50mM NaCl for the indicated protein or combination of proteins (at 10 μM each), imaged in the channel indicated at the top of the panel.

F. Enrichment ratio of OCT4-GFP versus GFP in MED1-IDR-mCherry droplets formed in droplet formation buffer without crowding agent at 50mM NaCl. $n > 20$, error bars represent the distribution between the 10th and 90th percentile.

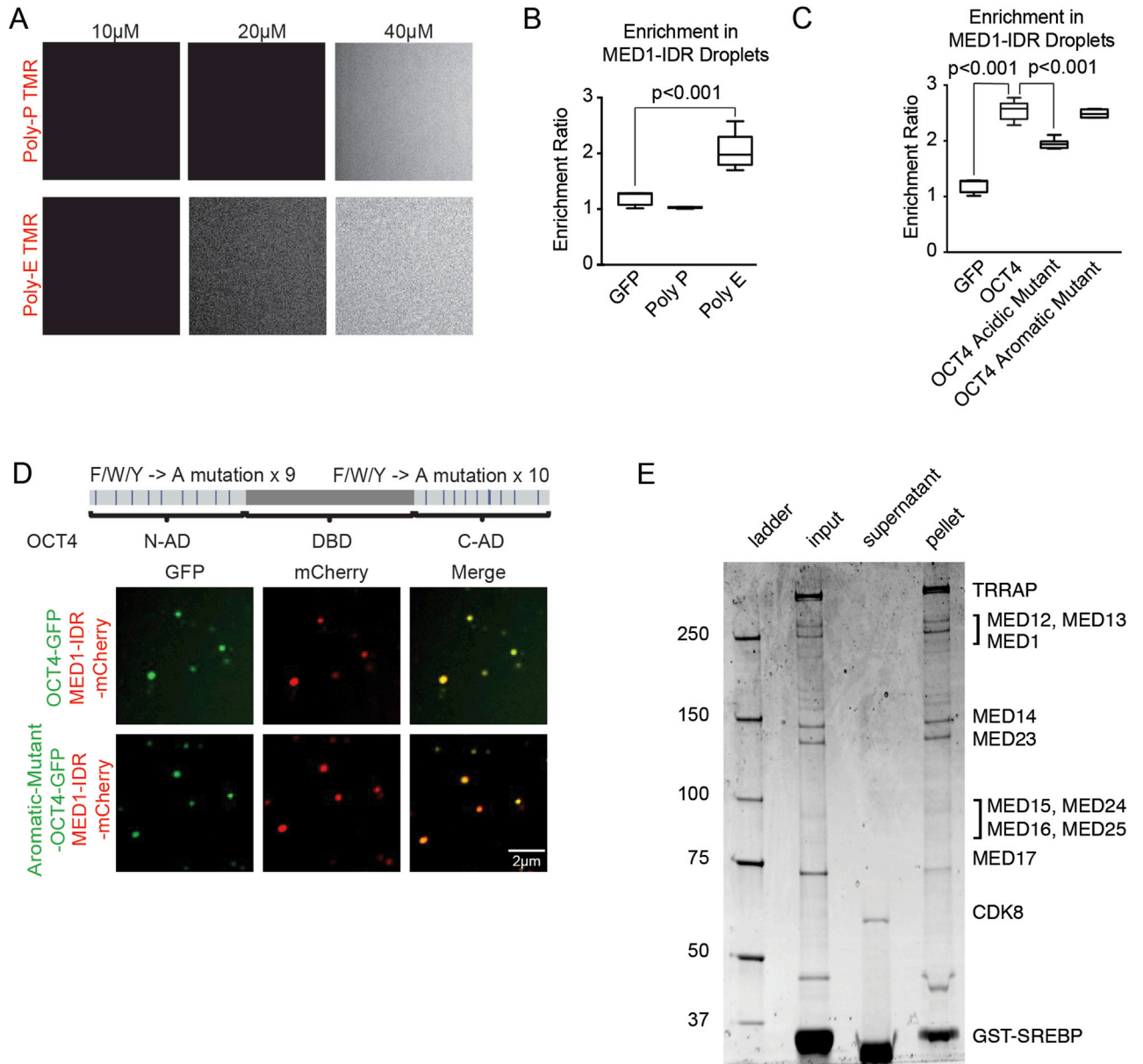


Figure S4. Phase Separation of Mutant OCT4, Related to Figure 4

A. Fluorescent microscopy of the indicated TMR-labeled polypeptide, at the indicated concentration in droplet formation buffers with 10% PEG-8000 and 125mM NaCl.

B. Enrichment ratios of the indicated polypeptide within MED1-IDR-mCherry droplets. $n > 20$, error bars represent the distribution between the 10th and 90th percentile.

C. Enrichment ratios of the indicated protein within MED1-IDR-mCherry droplets. $n > 20$, error bars represent the distribution between the 10th and 90th percentile.

D. (Upper panel) Schematic of OCT4 protein, aromatic residues in the activation domains (ADs) are marked by blue horizontal lines. All 9 aromatic residues in the N-terminal Activation Domain (N-AD) and 10 aromatic residues in the C-terminal Activation Domain (C-AD) were mutated to alanine to generate an OCT4-aromatic mutant. (Lower panel) Representative confocal images of droplet formation showing that the OCT4 aromatic mutant is still incorporated into MED1-IDR droplets. MED1-IDR-mCherry and OCT4-GFP or MED1-IDR-mCherry and OCT4-aromatic mutant-GFP were added to droplet formation buffers with 125mM NaCl at 10μM each with 10% PEG-8000 and visualized on a fluorescent microscope with the indicated filters.

E. Droplets of intact Mediator complex were collected by pelleting and equal volumes of input, supernatant, and pellet were run on an SDS-PAGE gel and stained with sypro ruby. Mediator subunits present in the pellet are annotated on the rightmost column.

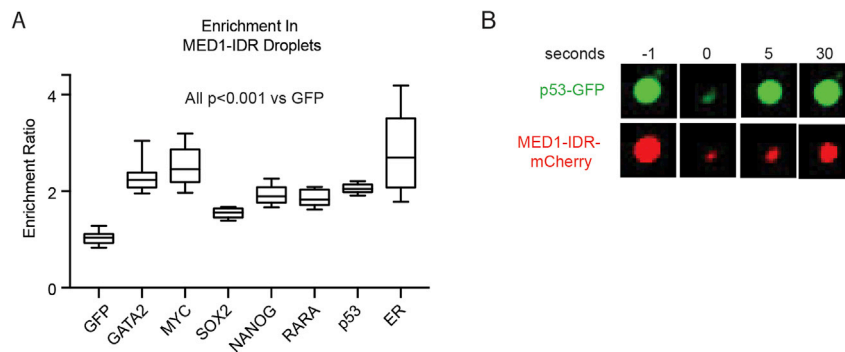


Figure S5. Diverse TFs Phase Separate with Mediator, Related to Figure 5

A. Enrichment ratios of the indicated GFP-fused TF in MED1-IDR-mCherry droplets. $n > 20$, error bars represent the distribution between the 10th and 90th percentile.

B. FRAP of heterotypic p53-GFP/MED1-IDR-mCherry droplets formed in droplet formation buffers with 10% PEG-8000 and 125mM NaCl, imaged every second over 30 s.

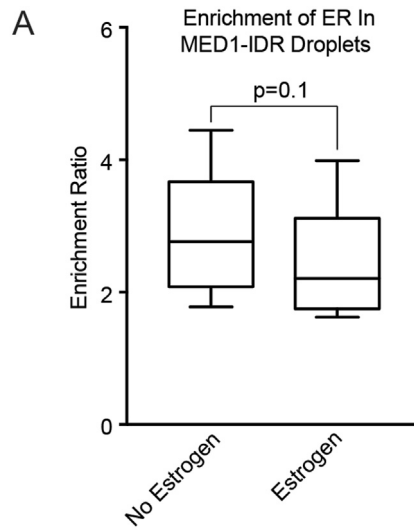


Figure S6. ER Phase Separates with MED1, Related to Figure 6

A. Enrichment ratio of ER-GFP in MED1-IDR-mCherry droplets in the presence or absence of 10uM estrogen. Droplets were formed in 10% PEG-8000 with 125mM NaCl. $n > 20$, error bars represent the distribution between the 10th and 90th percentile.

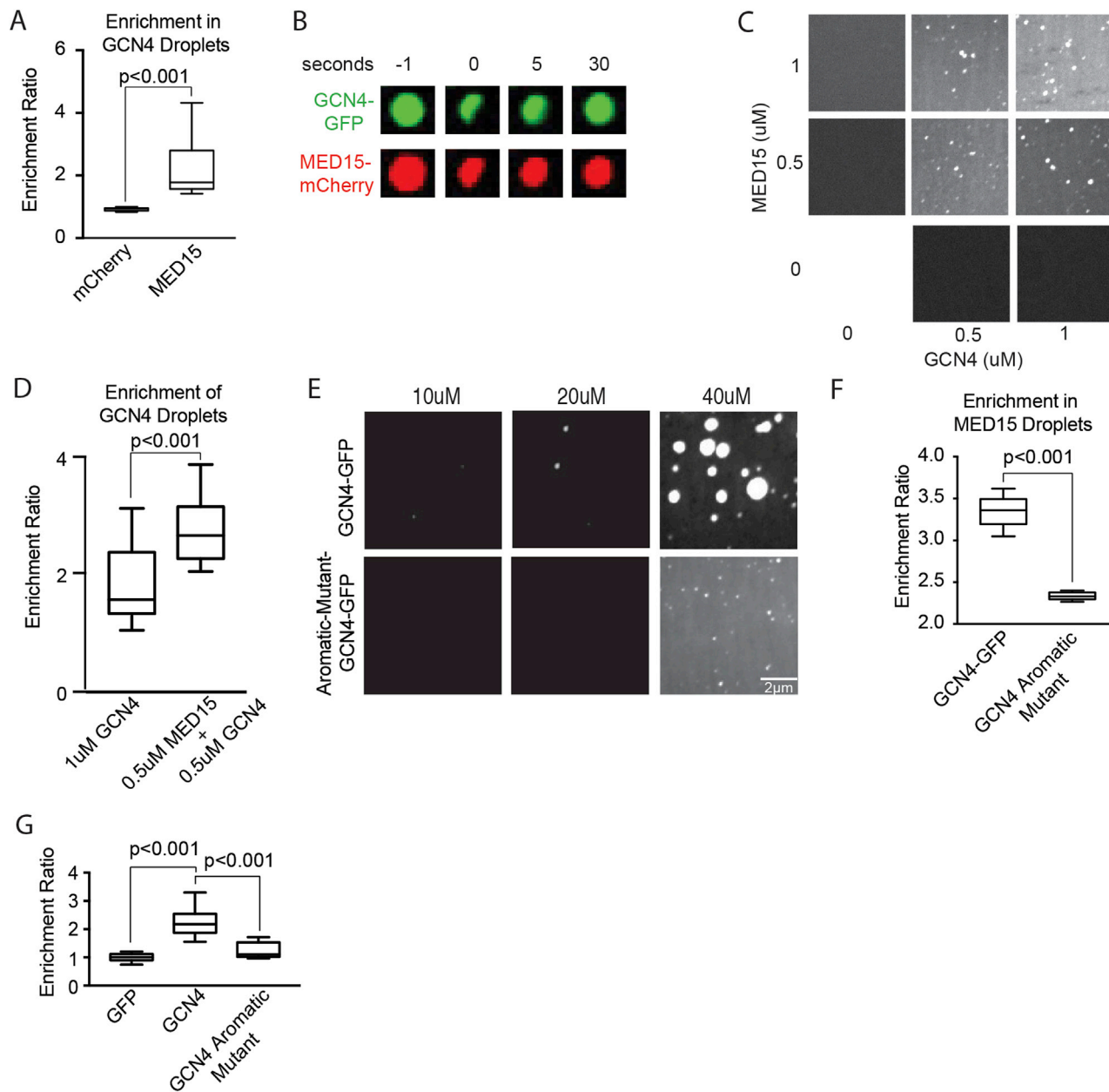


Figure S7. GCN4 and MED15 Form Phase-Separated Droplets, Related to Figure 7

A. Enrichment ratio of mCherry or MED15-mCherry in GCN4-GFP droplets, in droplet formation buffer with 10% PEG-8000 and 125mM NaCl. $n > 20$, error bars represent the distribution between the 10th and 90th percentile.

B. FRAP of heterotypic GCN4-GFP/MED15-IDR-mCherry droplets formed in droplet formation buffers with 10% PEG-8000 and 125mM NaCl, imaged every second over 30 s.

C. Phase diagram of GCN4-GFP and MED15-mCherry added at the indicated concentrations to droplet formation buffers with 10% PEG-8000 and 125mM salt.

D. Enrichment ratio of GCN4 droplets from S7C. $n > 20$, error bars represent the distribution between the 10th and 90th percentile.

E. Fluorescent imaging of GCN4-GFP or the aromatic mutant of GCN4-GFP at the indicated concentration in 10% PEG-8000 and 125mM NaCl. Shown are images from GFP channel.

F. Enrichment ratio of GCN4-GFP or the aromatic mutant of GCN4-GFP in MED15-mCherry droplets, formed in droplet formation buffer with 10% PEG-8000 and 125mM salt. $n > 20$, error bars represent the distribution between the 10th and 90th percentile.

G. Enrichment ratio of GFP, GCN4-GFP or GCN4-aromatic mutant-GFP in Mediator complex droplets. $n > 20$, error bars represent the distribution between the 10th and 90th percentile.